Modeling the formation and aging of secondary organic aerosols in Los Angeles during CalNex 2010

Patrick L. Hayes[1,2,3], Annmarie G. Carlton[4], Kirk R. Baker[5], Ravan Ahmadov[1,6], Rebecca A. Washenfelder[1,6], Sergio Alvarez[7], Bernhard Rappenglück[7], Jessica B. Gilman[1,6], William C. Kuster[6], Joost A. de Gouw[1,6], Peter Zotter[8], Andre S. H. Prévôt[8], Sönke Szidat[9], Tadeusz E. Kleindienst[5], John H. Offenberg[5], Jose L. Jimenez[1,2]

(1) Cooperative Institute for Research in Environmental Sciences (CIRES), University of Colorado, Boulder, CO, USA.
(2) Department of Chemistry and Biochemistry, University of Colorado, Boulder, CO, USA.
(3) Université de Montréal, Department of Chemistry, Montreal, QC, CANADA
(4) Department of Environmental Sciences, Rutgers University, New Brunswick, NJ, USA.
(5) US Environmental Protection Agency, Research Triangle Park, NC, USA.
(6) Earth System Research Laboratory, National Oceanic and Atmospheric Administration (NOAA), Boulder, CO, USA.
(7) Department of Earth and Atmospheric Sciences, University of Houston, TX, USA.
(8) Laboratory of Atmospheric Chemistry, Paul Scherrer Institute, Villigen, Switzerland.
(9) Department of Chemistry and Biochemistry & Oeschger Centre for Climate Change Research, University of Bern, Switzerland.

Correspondence to:
P. L. Hayes (patrick.hayes@umontreal.ca) and J. L. Jimenez (jose.jimenez@colorado.edu)

Abstract

Four different parameterizations for the formation and evolution of secondary organic aerosol (SOA) are evaluated using a 0-D box model representing the Los Angeles Metropolitan Region during the CalNex 2010 field campaign. We constrain the box model predictions with measurements from several platforms and compare predictions with particle and gas-phase observations from the CalNex Pasadena ground site. That site provides a unique opportunity to study aerosol formation close to anthropogenic emission sources with limited recirculation. The model SOA formed only from the oxidation of VOCs (V-SOA) is insufficient to explain the observed SOA concentrations, even when using SOA parameterizations with multi-generation oxidation that produce much higher V-SOA yields than have been observed in chamber experiments, or when increasing yields to their upper limit estimates accounting for recently reported losses of vapors to chamber walls. This finding is consistent with results from the Community Multiscale Air Quality (WRF-CMAQ) model (version 5.0.1), which provides excellent predictions of secondary inorganic particles species but underestimates the observed SOA mass by a factor of 25 when a VOC-only parameterization is used, and also with many previous model-measurement comparisons for pre-2007 anthropogenic SOA modules in urban areas.

Including SOA from primary semi-volatile and intermediate volatility organic compounds (P-S/IVOCs) following the parameterizations of Robinson et al. (2007), Grieshop et al. (2009), or Pye and Seinfeld (2010) substantially improves model/measurement agreement for mass concentration. When comparing the three parameterizations, the Grieshop et al. parameterization performs best and more accurately reproduces both the SOA mass concentration and oxygen-to-carbon ratio inside the urban area. Our results strongly suggest that other precursors besides VOCs, such as P-S/IVOCs, are needed to explain the observed SOA concentrations in Pasadena. All models over-predict SOA formation at long photochemical ages (≈3 days) compared to observations from multiple sites, which can lead to problems in regional and global modeling.

Among the explicitly modeled VOCs, the precursor compounds that contribute the greatest SOA mass are methylbenzenes. Polycyclic aromatic hydrocarbons (PAHs) are less important precursors and contribute less than 4% of the SOA mass. The amounts of SOA mass from diesel vehicles, gasoline vehicles, and cooking emissions are estimated to be 16 – 27%, 35 – 61%, and 19 – 35%, respectively, depending on the parameterization used, which is consistent with the observed modern carbon fraction of urban SOA, 71(±3)%. In-basin biogenic VOCs are predicted only a few percent contribution to SOA. A regional SOA background of approximately 2.1 $\mu g\ m^{-3}$ is also present due to the long distance transport of highly aged OA. The percentage of SOA from diesel vehicle emissions is the same, within the estimated uncertainty, as reported in previous work that analyzed the weekly cycles in OA concentrations (Hayes et al., 2013; Bahreini et al., 2012). However, the modeling work presented here suggests a strong anthropogenic source of modern carbon in SOA, due to cooking emissions, which was not accounted for in those previous studies.

Lastly, this work adapts a simple two-parameter model to predict SOA concentration and O/C from urban emissions. This model successfully predicts SOA concentration, and the optimal parameter combination is very similar to that found for Mexico City. This approach provides a computationally inexpensive method for predicting urban SOA in global and climate models. We estimate pollution SOA to account for 26 $Tg\ yr^{-1}$ of SOA globally, or 17% of global SOA, 1/3 of which is likely to be non-fossil.

1. Introduction

Submicron aerosols impact regional to global climate (IPCC, 2013), visibility (Watson, 2002), and human health (Dockery and Pope, 1994). Quantification of the environmental and health impacts of atmospheric aerosols is difficult however, because of our incomplete understanding of aerosol physical and chemical properties. Atmospheric aerosols are typically a mixture of organic and inorganic matter, and the organic fraction is normally composed of hundreds or even thousands of compounds. Due to this complexity, accurate prediction of OA concentrations, as well as chemical properties is challenging (Heald et al., 2011; Spracklen et al., 2011; McKeen et al., 2007). This problem is especially important given that OA represents roughly half of the total tropospheric submicron aerosol mass in many environments including polluted urban regions (Jimenez et al., 2009; Murphy et al., 2006).

Given its complexity, OA is often categorized based on sources. Primary organic aerosols (POA) are emitted directly into the atmosphere from sources such as motor vehicles, food cooking, and wildfires. SOA is formed in the atmosphere by photooxidation and/or heterogeneous or cloud processing of gas-phase precursors. The gas-phase precursors for SOA potentially have many sources including vehicle emissions, the biosphere, biomass burning, and food cooking (e.g. Bahreini et al., 2012; Hodzic et al., 2010b; Hallquist et al., 2009; Schauer et al., 1999). A large portion of the submicron OA throughout the world can be classified as SOA (Jimenez et al., 2009; Zhang et al., 2007). Even in urban areas such as the Los Angeles Metropolitan Area, SOA is often found to be larger than POA, especially in the summer (Hayes et al., 2013; Hersey et al., 2011; Docherty et al., 2008).

Traditional models for SOA formation use a semi-empirical approach wherein SOA formation is described in two steps: the gas-phase oxidation of VOC precursors resulting in the formation of semi-volatile organic compounds (SVOCs), followed by partitioning of the SVOCs to the particle phase. The parameters for these models (yields, saturation concentrations, etc.) are typically derived from smog chamber experiments on individual VOCs (Hallquist et al., 2009). Since about 2005, it has been shown in multiple publications from several field studies that traditional models under-predict observed SOA in urban areas by a large amount with a difference of up to a factor of 19. (Hodzic et al., 2010a; de Gouw and Jimenez, 2009; Dzepina et al., 2009; Volkamer et al., 2006). A similarly large underestimate is typically not observed in areas dominated by biogenic SOA (Slowik et al., 2010; Chen et al., 2009; Hodzic et al., 2009; Tunved et al., 2006). In response, new precursors and pathways for SOA formation have been identified from measurements and incorporated into SOA models. The new formation pathways include SOA formation from primary semivolatile and intermediate volatility organic compounds (P-S/IVOCs) (Robinson et al., 2007), aqueous phase production in clouds (e.g. Lim et al., 2005) and aerosols (Knote et al., 2014; Ervens and Volkamer, 2010), as well as the oxidation of VOCs such as isoprene, benzene, and acetylene that were previously thought to produce little or no SOA (Volkamer et al., 2009; Kroll et al., 2006; Martin-Reviejo and Wirtz, 2005).

The introduction of the volatility basis set (VBS) approach represents a conceptual advance for modeling OA (Donahue et al., 2006). This approach distributes organic species into logarithmically spaced volatility bins, which are used to calculate absorptive partitioning between the gas and particle-phases. Mass is transferred between the bins as photochemical oxidation proceeds and environmental parameters (i.e. temperature, dilution) change. The VBS has been applied to SOA from biogenic and anthropogenic VOC precursors as well as to P-S/IVOCs and the SOA formed from them (Tsimpidi et al., 2010; Robinson et al., 2007).

Although these updates have led to substantial reductions in the gaps between observed and predicted OA concentrations, major inconsistencies and uncertainties remain, and it is not clear that improved agreement is achieved for the right reasons. For instance, both Dzepina et al. (2011) and Hodzic et al. (2010a) reported that the Robinson et al. (2007) parameterization for the production of SOA from P-S/IVOCs contributed substantially to successful predictions of SOA in a box and a regional model for the Mexico City region, but the predicted O/C values were approximately a factor of 2 too low. A different parameterization of SOA from P-S/IVOCs published by Grieshop et al. (2009) led to overpredicted total SOA concentration, but successfully reproduced the measured O/C values.

Complicating the picture further was the additional finding in Dzepina et al. (2011) that if the VBS with multi-generational aging was applied to VOCs following Tsimpidi et al. (2010), then all the SOA mass could be successfully predicted without considering P-S/IVOCs. A similar finding was observed in Tsimpidi et al. (2010) wherein the inclusion of P-S/IVOCs and an "aging VBS" treatment of VOC oxidation worsened over-prediction in the model during the afternoon. Thus, the relative importance of P-S/IVOCs versus VOCs in urban SOA production remains very uncertain. More generally, achieving a robust model/measurement closure for the right reasons is critical for successful particulate matter pollution controls in urban areas.

Here we compare the results of a constrained SOA box model against measurements carried out at the Pasadena ground site during the California Research at the Nexus of Air Quality and Climate Change (CalNex) campaign. The use of a box model allows multiple state-of-the-art parameterizations to be tested. Once constrained by measurements, the box model facilitates the improved source apportionment of SOA in the Los Angeles Metropolitan Area. In particular, the importance of different precursors is quantitatively evaluated. Results are also compared to those of the 3-D WRF-CMAQ model. The importance of diesel versus gasoline emissions as sources of SOA precursors – a topic that has received much recent interest – is discussed as well (Hayes et al., 2013; Bahreini et al., 2012; Gentner et al., 2012). The CalNex field campaign, which took place in Spring/Summer 2010, provides a unique data set for evaluating SOA models because of the large scope of the campaign, and the generally clear-sky conditions during the campaign that limited the effects of cloud chemistry. Specifically at the Pasadena ground site, which operated from May 15 2010 to June 15 2010, there were over 70 gas and particle phase measurements including cutting-edge techniques that provide new insights into SOA sources and chemistry. For example, highly time resolved ^{14}C measurements with 3 – 4 h resolution are utilized in this work, whereas typically 12 h or lower resolution has been

reported (Zotter et al., 2014). By comparing the CalNex dataset to recently proposed SOA models, the research described below aims to evaluate recently proposed SOA models and assess the importance of different SOA sources and formation pathways.

2. Modeling methods

2.1. Pasadena ground site meteorology

An overview of the CalNex study has been recently published by Ryerson et al. (2013). The location and meteorology of the Pasadena ground site has been described in detail previously (Hayes et al., 2013; Washenfelder et al., 2011). Briefly, the site was located in the Caltech campus about 18 km northeast of downtown Los Angeles (34.1406 N, 118.1225 W). Pasadena lies within the South Coast Air Basin (SoCAB), and the Los Angeles metropolitan area. The prevailing wind direction during daytime in Pasadena was from the southwest, which brought air masses from the Santa Monica and San Pedro bays through Los Angeles to Pasadena. Thus, Pasadena during the daytime is predominately a receptor site for pollution emitted in the western Los Angeles metropolitan area that is then advected over a period of several hours (about 3 – 5 h). While more local emissions and background concentrations of atmospheric species must influence the site, the diurnal cycles of many primary species with anthropogenic sources, e.g. CO, black carbon (BC), benzene, appear to be dominated by advection of pollution from the southwest. Specifically, CO, BC and benzene concentrations display a strong peak a noontime as shown in Figure 2 of Hayes et al. (2013), which is due to a transport time of several hours until the emissions from the morning rush hour arrive in Pasadena. At nighttime, winds were weak and were most frequently from the southwest or southeast, which is illustrated in the supporting information (Figure A-2) of Hayes et al. (2013). The site was influenced at that time by more local emissions than by advection from the downtown Los Angeles. Aged emissions from the prior daytime may have influenced the site as well during nighttime.

2.2. SOA box model

The models in this work are summarized in Table 2. The box model used here accounts for SOA formed from gas-phase oxidation of two sets of precursors: (1) VOCs, and (2) P-S/IVOCs. Also included in the total model SOA is background SOA (BG-SOA), with a constant concentration of 2.1 μg m^{-3} that is derived from observations as described later in Section 2.4. BG-SOA is considered non-volatile in the model, which is consistent with observations that very aged SOA has low volatility (Cappa and Jimenez, 2010). For the remainder of the SOA the equilibrium partitioning between the particle and gas-phases is calculated using the reformulation of Pankow Theory by Donahue et al. (2006). The particle-phase fraction of species *i*, ξ_i, is calculated using its effective saturation concentration, C_i^*, and the total concentration of the organic material available for partitioning, *[OA]*.

$$\xi_i = \left(1 + \frac{C_i^*}{[OA]}\right)^{-1} \; ; \; [OA] = \sum_i [P\text{–}S/IVOC]_i \, \xi_i \qquad (1)$$

We note that there is ongoing scientific research examining if OA adopts a liquid or solid/glassy phase with potentially slow diffusion properties, and the conditions that result in equilibrium or kinetically-limited partitioning are not yet clear (e.g. Perraud et al., 2012; Cappa and Wilson, 2011). For the purpose of this study however, field measurements from CalNex strongly suggest that organic aerosols undergo equilibrium partitioning in Pasadena (Zhang et al., 2012). In particular, for water-soluble organic carbon, a surrogate for SOA, the partitioning coefficient was observed to be correlated with the OA mass. A similar observation was made at a rural site in Colorado, USA, and the lack of kinetic limitations to equilibrium may be attributable to the higher ambient relative humidity, mostly greater than 30%, in both Pasadena and Colorado compared to some studies that have reported kinetic limitations (Yatavelli et al., 2014). Furthermore, we note that the diurnally averaged relative humidity in Pasadena was always greater than 60%, which laboratory studies have suggested is the threshold above which particles form liquid phases (Saukko et al., 2012).

V-SOA in the box model includes products from the oxidation of 46 VOCs, and the V-SOA mass is distributed into a 4-bin VBS as shown Figure 1 (C^*=1, 10, 100, or 1000 μg m^{-3}). Furthermore, a table with the names of each VOC as well as the relevant model parameters is provided in the supporting information (Table SI-1). The reaction rates for most of the VOCs are taken from Atkinson and Arey (2003) and, when not available there, Carter (2010). Three terpene compounds (α-pinene, β-pinene, and limonene) were lumped for this model, and the rate constant of this lumped precursor species is the weighted average – by ambient concentrations – of the individual rate constants (Atkinson and Arey, 2003). In addition, the rates for naphthalene, 1-methylnaphthalene, and 2-methylnaphthalene oxidation are taken from Chan et al. (2009). The SOA yields for the VOCs are taken from Tsimpidi et al. (2010). For naphthalene and the methylnaphthalenes the yields are from data presented in Chan et al. (2009), which have been re-fitted to obtain yields for the 4-bin VBS utilized in this work. V-SOA is also allowed to 'age' after the initial reaction, and the subsequent gas-phase oxidation leads to a 10× decrease in volatility as well as a 7.5% increase in mass due to added oxygen for each generation.

SOA from P-S/IVOCs (SI-SOA) is simulated utilizing three different parameter sets. No duplication of precursors is expected between the Tsimpidi et al. (2010) parameterization and the three P-S/IVOCs parameterizations, with the possible exception of the naphthalenes (Dzepina et al., 2011; Dzepina et al., 2009; Robinson et al., 2007). However, since the naphthalenes contribute a small amount to the total SOA mass, the impact of double-counting their SOA contribution is negligible. The first two P-S/IVOCs parameterizations are from Robinson et al. (2007), hereinafter "ROB", and an alternate set published by Grieshop et al. (2009), hereinafter "GRI". The differences between the two parameterizations are highlighted in Figure 1. When compared to ROB, primary and secondary species in GRI have a lower gas-phase reactivity (2×10^{-11} versus 4×10^{-11} cm^3 $molec^{-1}$ s^{-1}), a larger decrease in volatility per oxidation step (two orders of magnitude versus one), and more oxygen mass added to the products (40% versus 7.5% of the precursor mass). Furthermore, there are differences in the assumed enthalpies of

vaporization, ΔH_{vap}, and molecular weights. Details of both parameterizations are given in Table SI-2 in the supporting information.

The third parameterization utilized for SI-SOA is that published by Pye and Seinfeld (2010), hereinafter "PYE", which is also illustrated in Figure 1. In PYE the SOA from primary SVOCs and primary IVOCs follow different treatments. The primary SVOCs emitted are represented by two lumped species with C^*=20 and 1646 μg m^{-3} and relative concentrations of 0.51 and 0.49, respectively. The gas phase reactivity (2×10^{-11} cm^3 $molec^{-1}$ s^{-1}) and decrease in volatility per oxidation step (two orders of magnitude) is identical to GRI. However, only one oxidation step is allowed in PYE. The oxygen mass added to the products is 50% of the precursor mass, which is higher than that for ROB and GRI. Another difference in PYE is the enthalpy of vaporization for all organic species, which is 42 kJ/mol. Lastly, the molecular weight utilized here is 250 g mol^{-1}, the same as GRI, although this parameter is not specified in Pye and Seinfeld (2010). In PYE also the concentration of SOA from primary IVOCs is estimated by scaling-up the concentration of SOA from naphthalene by a factor of 66.

Heterogeneous uptake of glyoxal onto aerosols can be a relevant source of SOA under some conditions (Dzepina et al., 2009; Volkamer et al., 2007). Previously published work on the glyoxal budget for CalNex indicates that this compound contributes only a small fraction of the SOA mass in the LA basin, however (Knote et al., 2014; Washenfelder et al., 2011), and we do not consider it further in this study. In Pasadena, the urban SOA peaked in the afternoons, which were generally clear and sunny during the campaign. This observation is consistent with the conclusion that reactions occurring in clouds did not play a major role in SOA production during CalNex. In addition, a comparison of OA/ΔCO for three days that were cloudy against the remainder of the campaign shows no apparent difference in the magnitude of the ratio or its evolution with photochemical age (Figure SI-1), which further supports the conclusion that SOA production from clouds can be neglected in this study.

The design of the model used here includes several more elements that are general for V-SOA and SI-SOA. Only oxidation by hydroxyl radical (•OH) is considered since in urban regions other oxidants such as ozone, nitrate radical, and chlorine radical are expected to be minor contributors to SOA formation from urban VOCs (Hayes et al., 2013; Dzepina et al., 2011; Dzepina et al., 2009). Additionally, the model is run using "high-NO_x conditions," which is consistent with previously calculated branching ratios for the RO_2 + NO, RO_2 + HO_2, and RO_2 + RO_2 reactions (Hayes et al., 2013) and the dominance of the RO_2 + NO pathway. The primary and secondary species are assumed to mix into a single organic phase. This assumption is based on observations made off the coast of California that SOA condenses on primary particles (e.g., BC and POA) as indicated by the similar size distributions for these species across a range of photochemical ages (Cappa et al., 2012). In addition, the organic phase is taken to be separate from the inorganic phases, which is consistent with the relatively low O:C values observed during CalNex (Hayes et al., 2013) and previous studies demonstrating that organic/inorganic phase separation occurs when O:C is less than 0.7 (Bertram et al., 2011). It should be noted that

this statement holds true even after applying the updated calibration for AMS O:C (Canagaratna et al., 2014).

The temperature dependence of C^* is calculated with the Clausius-Clapeyron equation.

$$C_i^* = C_{i,o}^* \frac{T_0}{T} \exp\left[\frac{\Delta H_{vap}}{R}\left(\frac{1}{T_o} - \frac{1}{T}\right)\right] \qquad (2)$$

Where $C_{i,o}^*$ is the effective saturation concentration of condensable compound i at the reference temperature T_o (K), and R is the ideal gas constant. The ambient temperature, T, was taken to be 18°C, which represents the average campaign temperature during CalNex. A sensitivity test exhibited less than a 4% change in predicted mass at a given time-of-day when using 14°C and 24°C, which are the minimum and maximum temperatures for the diurnal cycle. The error in predicted mass over this temperature range is small compared to other uncertainties in SOA modeling, and therefore the use of a constant temperature of 18°C to calculate C* should introduce negligible errors.

2.3. Model set-up

This work utilizes a box approach wherein the model calculates the evolution of organic species in an air parcel as it undergoes photochemical aging. The calculation is run 24 times to predict the average diurnal cycle for the entire campaign (15 May – 15 June). The initial concentrations of VOCs in the air parcel are calculated by multiplying the background-subtracted CO concentrations measured at Pasadena by the emission ratios (ΔVOC/ΔCO) previously determined for CalNex, which are consistent with those for other US urban areas (Borbon et al., 2013; Warneke et al., 2007). CO is an inert tracer of combustion emissions over these timescales and its formation from VOCs is very minor as well (Griffin et al., 2007). The CO background level represents the amount present from continental-scale transport and for which the co-emitted organic species have been lost by deposition (e.g. DeCarlo et al., 2010). The background was determined by examining CO measurements taken aboard the NOAA WP-3D aircraft off the Los Angeles coastline at altitudes less than 200 m as described in our previous paper (Hayes et al., 2013). Given that the model is set-up to predict the mean diurnal cycle of SOA during the entire CalNex-Pasadena measurement period, the mean diurnal cycle of the CO concentration is used for the calculation of the emissions. An important advantage of using CO as a conserved urban emissions tracer is that dilution of emissions in the air parcel is implicitly included in the model, since the reductions in CO concentration at the site will lead to lower calculated initial precursors concentrations in that air parcel.

The model consistency with the VOC measurements is evaluated by comparing the measured and modeled diurnal cycles. The cycles are given in Figure SI-2. It is observed that the model is consistent with the VOC measurements.

For naphthalene and its analogs, emission ratios are not available in the literature, to our knowledge. To obtain the emission ratios the concentrations of the polycyclic aromatic hydrocarbons were plotted versus CO, and a linear orthogonal distance regression ODR analysis was carried out. The data were filtered and include only periods from 00:00 – 06:00 (local time) to minimize depletion by photochemical processing (Figure SI-3). The slope from the regression analysis was then used as the emission ratio. However, as observed in Figure SI-3, the diurnal cycles for naphthalene and its analogs are not well-reproduced by the model during the daytime when using the early morning emission ratios. The sampling of these compounds was performed on a tar roof, and it is possible that the local concentrations in the vicinity of roof may be elevated during daytime due to volatilization of the roofing tar and not representative of concentrations throughout the Los Angeles basin. The naphthalene and methylnaphthalene concentrations are well correlated with temperature. However, it is also possible that the volatilization occurs over a larger city scale, and thus a variation of the model is run wherein the emission ratios are changed empirically along the diurnal cycle so that the model reproduces the measured diurnal cycle for each speciated naphthalene (Figure SI-3). The increases in emissions in the afternoon range between 1 and 3.5 times the original value, and the implications for SOA are discussed in Section 3.1.3.

The calculation of the initial P-S/IVOC concentrations requires a somewhat different procedure since the emissions ratios with respect to CO are not known. Instead, the amount of initially emitted POA is calculated from measured ΔPOA/ΔCO ratios and the measured CO concentration in Pasadena. Then the total concentration of P-S/IVOCs is set so that the particle-phase P-S/IVOC concentration matches the amount of initially emitted POA, while constraining the volatility distribution to that of the corresponding parameterization, as done in previous studies (e.g. Dzepina et al., 2009).

The model consistency with respect to the POA measurement is shown in Figure SI-2. The comparison for POA is adequate, and a linear ODR analysis yields a slope of 1.01 (R = 0.76) when the GRI parameterization is used. Of the three models for SI-SOA, PYE shows a larger positive bias. This is likely due to the relatively large amount of primary SVOCs placed in the C*=20 bin compared to ROB and GRI, which will result in more partitioning to the particulate phase as the total OA mass is increased (e.g. by SOA formation)

The initial VOCs and P-S/IVOCs are then oxidized in the air parcel with the amount of oxidation set to match the photochemical age measured at Pasadena at each time of the day. The aging of the air parcel is simulated separately 24 times with each simulation using measured parameters (i.e. ΔCO, photochemical age, POA) corresponding to one hour during the mean diurnal cycle. Following Dzepina et al. (2009) the evolution of the different compounds in each of the 24 aging simulations is calculated by discretizing the rate equations using Euler's method.

The photochemical age of the urban emissions at each time of the day is determined from the ratio of 1,2,4-trimethylbenzene to benzene as described previously (Hayes et al., 2013; Parrish et al., 2007). We note that the photochemical age estimated from NO_x/NO_y is very similar (Hayes et al., 2013), which is consistent with previous results from Mexico City for ages

shorter than 1 day (C. A. Cantrell, Univ. of Colorado, personal communication, 2014). There are three important considerations that must be evaluated when using VOC concentration ratios as photochemical clocks.

First, trimethylbenzene and benzene are predominately from anthropogenic sources, and thus the photochemical clock only applies to the evolution of anthropogenic emissions. Previous work by Washenfelder et al. (2011) estimated that most biogenic VOCs were emitted mostly in the last quarter of the trajectory of the air parcel arriving at Pasadena at 16:00 PDT. This estimate was based on the vegetation coverage observed in visible satellite images of the upwind areas, as well as on the ratio of isoprene to its first-generation products (methyl vinyl ketone and methacrolein). However, in this work, the photochemical age for biogenic VOCs is kept the same as for the anthropogenic VOCs. This approach will overestimate the amount of photochemical aging – and the SOA from in-basin biogenic emissions – during daytime. The modeled biogenic SOA should thus be considered an upper limit. The emissions of biogenic VOCs were adjusted empirically to match the observed concentrations of isoprene and terpenes, after accounting for anthropogenic isoprene using Δ(isoprene)/ΔCO (Borbon et al., 2013). Only ~4% of the daily average isoprene is from anthropogenic sources. As discussed below, the amount of SOA from in-basin biogenic VOCs is very small. Thus, our SOA model results are not sensitive to the details of how SOA from biogenic VOCs emitted within the LA basin is modeled. We do not include oxidation of biogenic VOCs by O_3 or NO_3 in the box model, but these oxidants have only a minor role in SOA formation during the daytime when the peak for in-basin SOA concentration is observed. In particular, given the measured concentrations of oxidants (Hayes et al., 2013), oxidation of isoprene and terpenes by OH is 37 and 5 times faster on average, respectively, than oxidation by O_3 during daytime.

The second consideration is that the photochemical ages used here (Figure 2) are calculated using an average OH concentration of 1.5×10^6 molec cm^{-3}. The model is run with the same concentration, which is necessary to match the model and observed OH exposure. (OH exposure is the concentration integrated over time for an air parcel.) Thus in the middle of the day the photochemical age will be longer than the transport age, and the opposite will be true during periods with low ambient OH.

Third, photochemical age is a quantity developed as a metric for parcels of air arriving at a remote receptor site, and it is derived by assuming that the parcel is decoupled from fresh emissions as it is transported (Kleinman et al., 2007; Parrish et al., 2007). However, Pasadena is not a remote receptor site, and it is impacted by pollution that has been emitted recently as well as transported from more distant locations. The error in the calculated photochemical age that results from the mixing of nearby and far sources is evaluated in our previous work, and it may lead to underestimation of the actual photochemical age by ~10% (Hayes et al., 2013), which is relatively minor compared to the uncertainty in the OA measurement of ±30% (Middlebrook et al., 2012) and possible biases in the different SOA parameterizations.

2.4. Model/measurement comparisons

The model inputs are the following: the mean diurnal cycles for photochemical age, POA, and CO concentration (after subtracting the CO background), as well as a constant temperature and BG-SOA concentration. The model is then compared against the average diurnal cycles of various OA properties (e.g. concentration, O:C). The measurements utilized in this study are summarized in Table 3. In previous work the concentrations of five different OA components were determined using positive matrix factorization (PMF) of aerosol mass spectrometer (AMS) data, and the diurnal cycles of these components are shown in Figure 2 (Hayes et al., 2013). Hydrocarbon-like organic aerosol (HOA) and cooking-influenced organic aerosol (CIOA) are both thought to be dominated by POA. As discussed in Hayes et al. (2013), HOA is dominated by vehicle combustion emissions, and the CIOA is dominated by cooking sources. Low volatility oxygenated organic aerosol (LV-OOA) is a surrogate for highly aged secondary organic aerosol, and it displays a flat diurnal profile. Furthermore, recent ^{14}C measurements show that this component is largely composed of non-fossil carbon (Zotter et al., 2014). Both of these observations indicate that LV-OOA is transported into the Los Angeles Basin (Hayes et al., 2013).

Results from 3-D WRF-Chem simulations were also used to evaluate the concentration of BG-SOA. These simulations determined the BG-SOA by removing all the emissions in the Los Angeles region as shown in Figure SI-4, and it was observed that there are both biogenic and anthropogenic emissions in California that contribute to the background OA. In addition, background marine OA is thought to be very low during the CalNex measurement period, since concentrations of OA were less than 0.2 μg m^{-3} over the open ocean west of California for regions with low pollution influence (P. K. Quinn, NOAA, personal communication, 2012). As shown in Figure 2B, the background SOA concentration from the WRF-Chem simulation is similar to the concentration of LV-OOA. Given these observations as well as the ^{14}C results discussed in the previous paragraph, we use the LV-OOA component to constrain the amount of BG-SOA, and specifically, set the amount of BG-SOA to be the minimum of LV-OOA observed in the diurnal cycle (2.1 μg m^{-3}).

In contrast, semi-volatile oxygenated organic aerosol (SV-OOA) displays a distinct diurnal profile that peaks at a similar time as photochemical age, which is consistent with this component being a proxy for freshly formed SOA from urban emissions. The ^{14}C measurements also indicate that SV-OOA is predominately, 71% (±3%), composed of fossil carbon. (Note: to obtain this percentage it is assumed that the OC/OM ratio is the same for fossil and non-fossil SV-OOA.) As described above, the box model designed here is specifically focused on SOA formation from precursors emitted within the Los Angeles basin, and the ^{14}C measurements and diurnal cycle strongly indicate that SV-OOA concentration is a better surrogate of total urban SOA than the total OOA concentration. Lastly, there is a fifth component displayed in Figure 2B, local organic aerosol (LOA) of primary origin and of uncertain sources, but this component comprises only ~5% of the aerosol mass. It is thought to be emitted very close to the site based on its very rapid time variations, and thus any co-emitted VOCs or S/IVOCs would have very

little time to react and form SOA. Therefore LOA is not considered further in this modeling study.

In principle, the box model could be run for multiple individual days. However, some datasets and published results used in this study are not available with sufficient time resolution for such an approach. In particular, the thermal desorption gas chromatograph mass spectrometry analysis for naphthalenes required filter samples that were composited over several days. In addition, both the apportionment of the SV-OOA and LV-OOA components between fossil and non-fossil sources (Zotter et al., 2014) as well as the analysis of the diesel fraction of OOA (Hayes et al., 2013) required analyzing datasets from multiple days as a single ensemble. To facilitate incorporating these datasets and published results into this study, we have chosen to run the box model so that it simulates the average diurnal cycle during the campaign. The measurements used here (Table 3) all had excellent coverage during the CalNex campaign, with each instrument reporting data for more than 75% of the total campaign duration. Thus, the measurements are expected to be representative of conditions during the campaign. An exception is the ^{14}C measurements, which were carried out on filters collected over 7 days. This limited sampling period is due to the time and resource intensive nature of the ^{14}C measurements (Zotter et al., 2014).

2.5. Modeling the SOA oxygen content

To simulate the O:C ratio of total OA, the box model utilizes the measured O:C ratios for HOA, CIOA, and LV-OOA. The O:C ratios of HOA and CIOA are assumed to be constant because they are primary aerosols whose heterogeneous aging is relatively slow, and thus their O:C ratios should only vary by a relatively small amount (Donahue et al., 2013). LV-OOA is predominately composed of aged background OA, and thus its O:C ratio should not vary substantially either. The oxygen and carbon mass from HOA, CIOA, and LV-OOA are then added to the oxygen and carbon mass predicted in the model for freshly formed SOA.

The O:C ratio of V-SOA is simulated using a modified version of the approach described in Dzepina et al. (2009). In that previous work the O:C of V-SOA was estimated to be 0.37 and constant. While this estimate is consistent with chamber experiments of aromatic precursors, it is conceptually difficult to reconcile with V-SOA aging wherein successive oxidation reactions are expected to reduce volatility and increase O:C. It is therefore assumed in the box model that O:C increases as follows: $C^* = 1000$ µg m^{-3}, O:C = 0.25; $C^* = 100$ µg m^{-3}, O:C = 0.30, $C^* = 10$ µg m^{-3}; O:C = 0.4; $C^* = 1$ µg m^{-3}, O:C = 0.60. This O:C distribution is taken from the first-generation distribution of Murphy et al. (2011), and in that work the O:C ratio was simulated in a full 2-D VBS and depends on both volatility bin as well as oxidation generation. For the purpose of this study an intermediate approach is used where O:C depends on volatility bin only, and the first-generation distribution of Murphy et al. (2011) is applied to all oxidation generations of SOA.

The O:C ratio for SI-SOA is simulated following the approach described in Robinson et al. (2007). Conceptually, with each oxidation step the model adds 1 oxygen atom per 15 carbon

atoms for ROB and 5.3 oxygen atoms per 15 carbons for GRI. This oxidation then gives an increase in mass of 7.5% or 40% for ROB and GRI, respectively, as discussed previously. (Note: It is assumed that H = 2×C + 2, which may not be strictly true, but an error of 1 or 2 hydrogen atoms per carbon does not substantially alter the calculated values for the mass increase.) With this relationship O:C can be calculated for each generation of oxidation, and the OM:OC ratio can be calculated as well using the relationship OM:OC = 1 + (16/12)×O:C + (1/12)×H:C, in which H:C = 2 – 0.54×O:C (Canagaratna et al., 2014; Hayes et al., 2013; Murphy et al., 2011). Then the OM:OC ratio is used to convert the OM mass concentration in each generation bin to OC mass concentration, and the O:C ratio is used to convert the OC mass in each generation bin to O mass concentration. Finally, the O mass and OC mass are each summed and subsequently divided to obtain O:C.

2.6. Correction for changes in partitioning due to higher OA concentrations upwind of Pasadena

To account for changes in partitioning due to lower planetary boundary layer (PBL) heights, and thus, increased particle concentrations upwind of Pasadena, the concentrations of POA, V-SOA, and SI-SOA are increased upwind of Pasadena beyond the amount already simulated in the model. This correction is necessary because using CO as a conservative tracer of emissions does not account for how particulate concentration influences partitioning upwind of Pasadena. The correction of the partitioning mass is estimated using three different methods depending on the time-of-day. First, for air parcels measured at 00:00 – 07:00 local time when the PBL height is essentially constant for an extended period and emissions are dominated by local sources (Hayes et al., 2013), no correction needs to be made. Second, for air parcels measured between 07:00 – 16:00 when the PBL is increasing as the air parcels are advected, a correction is applied that assumes the PBL increases linearly from the height measured in the early morning hours to the height measured for a given time of day. Third, for air parcels after 16:00, it is assumed that a residual layer aloft is decoupled from the ground after 16:00, resulting in no subsequent dilution.

The correction for the partitioning calculation described in the previous paragraph is an approximation, and two sensitivity studies are carried out to estimate the magnitude of the possible errors introduced by this approximation. The first study follows the approach described above, except that instead of linearly increasing the partitioning mass upwind of Pasadena the correction follows a step-function and increases the partitioning mass to its maximum value immediately upwind of the ground site. This test should overestimate the amount of partitioning to the particle-phase, since such a dramatic change in PBL height is not expected. The second sensitivity study simply applies no correction factor to the partitioning mass, and thus it underestimates the partitioning to the particle-phase. For the model runs with the ROB and GRI parameterizations the resulting changes in average predicted mass for the sensitivity studies are +4/-12% and +6/-7%, respectively. These changes are small, which indicates that the description of the boundary layer dilution does not have a major influence on the results.

2.7. WRF-CMAQ model runs

The Community Multiscale Air-Quality Model (WRF-CMAQ) version 5.0.1 (https://www.cmascenter.org/cmaq/) was applied with 4 km horizontal grid resolution and 34 vertical layers extending from the surface (layer 1 height ~38 m) to 50 mb for the time period matching the CalNex field campaign. Aqueous phase chemistry includes oxidation of sulfur and methyglyoxal (Sarwar et al., 2013; Carlton et al., 2008), gas phase chemistry is based on Carbon-Bond 05 with updates to toluene reactions (Yarwood, 2010), and inorganic chemistry is based on the ISORROPIA II thermodynamic model (Fountoukis and Nenes, 2007). WRF-CMAQ estimates SOA yields from VOC precursors including isoprene, monoterpenes, sesquiterpenes, xylenes, toluene, benzene, and methylglyoxal (Carlton et al., 2010). Note that WRF-CMAQ contains the SOA precursor species alkanes and glyoxal, but these are not explicit species in the CB05-TU gas phase mechanism (e.g., alkanes are mapped to "PAR", or paraffins). SOA species oligomerize to non-volatile organic carbon grouped by anthropogenic and biogenic origin (Carlton et al., 2010).

The Weather Research and Forecasting model (WRF), Advanced Research WRF core (ARW) version 3.1 (Skamarock et al., 2008) was used to generate gridded meteorological fields used for input to WRF-CMAQ and the emissions model. Surface variables, flow patterns, and daytime mixing layer heights are generally well characterized during this time period (Baker et al., 2013). Hourly solar radiation and surface layer temperature estimated by the WRF model are used as input for the Biogenic Emission Inventory System (BEIS) version 3.14 to estimate hourly speciated VOC and NO_x emissions (Carlton and Baker, 2011).

Stationary point source emissions are based on continuous emissions monitor (CEM) data for 2010 where available and otherwise the 2008 version 2 National Emission Inventory (NEI). Area source emissions are also based on the 2008 version 2 NEI. Mobile sector (on-road and off-road) emissions are interpolated between 2007 and 2011 totals provided by the California Air Resources Board. Emissions from other areas of the United States and other countries are included through time and space variant lateral boundary inflow. Hourly boundary inflow concentrations are taken from a coarser WRF-CMAQ simulation covering the continental United States that used inflow estimates from a global GEOS-CHEM (version 8.03.02) model (http://acmg.seas.harvard.edu/geos/) simulation. Additional details regarding model setup and evaluation are provided elsewhere (Kelly et al., 2014).

2.8. WRF-Chem model runs

Weather Research and Forecasting Model coupled to Chemistry (WRF-Chem) is a fully coupled meteorology-chemistry model. WRF-Chem simulations were performed for May and June 2010 on a 12 km resolution domain, which covers a large part of the western United States. The model simulations include meteorological, gas, and aerosol phase chemical processes. The SOA scheme used in this study is based on the VBS approach. The SOA parameterization is described in detail by Ahmadov et al. (2012). Here the main objective of the WRF-Chem simulation was to estimate the OA contribution of the emission sources located upwind of the

Los Angeles basin. Thus, all the anthropogenic emissions and biogenic VOC fluxes were set to zero over an area of 60 x 72 km covering the Los Angeles basin (Figure SI-4) in our simulation. The WRF-Chem simulated OA concentrations for the Pasadena site therefore provide an estimate of the BG-OA at this site.

3. Results and discussion

3.1. Modeling urban SOA mass concentration

3.1.1. Urban SOA concentration: model versus measurement comparisons

In Figure 3 the diurnal cycles of SV-OOA and urban SOA are shown. For all the model variations, the model V-SOA (light blue area) is substantially smaller than the observed SV-OOA concentrations (solid black line), even though additional partitioning mass of SI-SOA is available for all model runs. It is possible that the SOA yields used for V-SOA, which are based on the chamber experiment literature, are several-fold too low due to, for example, losses of gas-phase species to chamber walls (Zhang et al., 2014; Matsunaga and Ziemann, 2010). To investigate this possibility a model variation – named "ROB + 4xV" – is run where the SOA yields from aromatics are increased by a factor of four, based on recent chamber studies in which higher concentrations of aerosol seed were utilized in order to suppress losses to chamber walls, and an upper limit of a factor of 4 increase in V-SOA yield was estimated (Zhang et al., 2014). The aging of secondary species produced from VOCs is turned off in that variation. The corresponding result is also shown in Figure 3. Even in this model variation where the V-SOA concentrations are substantially higher, additional SOA precursors must be included to achieve model/measurement closure. This result is also true despite the inclusion of full V-SOA aging in ROB, GRI, and PYE, which increases the amount of SOA from VOCs to levels far beyond those observed in chambers, although over longer timescales than for the 4xV case. Previous work modeling SOA in Mexico City showed that either V-SOA aging or SI-SOA must be included in models to match observed SOA concentrations, but the inclusion of both resulted in an over prediction (Dzepina et al., 2011; Tsimpidi et al., 2010). In this study, the inclusion of aging only increases the concentration of V-SOA by 8 – 45% depending on the time of day due to the relatively low experimental photochemical ages. Thus, by testing models of SOA formation at short ages, our case study points towards the importance of additional SOA precursors such as P-S/IVOCs.

When comparing the four parameterizations for SOA formation, it is apparent that the GRI and ROB + 4xV variations best reproduce the observations. The predicted SOA mass using GRI lies within the measurement uncertainty most of the day. In contrast, the ROB variation does not produce high enough concentrations of SOA, and the model is consistently lower than the measurements even after considering the measurement uncertainties. The PYE variation tends to over predict SOA concentrations especially at nighttime, and also exhibits larger discrepancies with respect to measured POA concentrations (Figure SI-2). Finally, the performance of the ROB + 4xV variation is similar to GRI, highlighting the uncertainties about the dominant SOA precursors in urban areas.

In general, the measurements peak one hour later than the model, which may be due to the simple treatment of sources and transport in the modeled air mass, but the overall correlation is excellent: R = 0.93 - 0.94 for ROB, GRI, PYE, and ROB + 4xV. This study contrasts with an earlier comparison of the ROB and GRI parameterizations for SOA in Mexico City, which showed that GRI produces more SOA than observed (Dzepina et al., 2011). Although the same modeling method was used to quantify the emissions and properties of P-S/IVOCs in both studies, the sources, composition, and SOA yields of P-S/IVOCs in urban areas are poorly characterized, and differences in those between the two urban areas may explain the differences in model performance for Pasadena and Mexico City.

3.1.2. Total SOA concentration: fossil vs contemporary carbon

As described above, on average 71(±3)% of the SV-OOA is composed of fossil carbon (Zotter et al., 2014), and it is important to evaluate whether this percentage is consistent with the model results. As shown in Figure 3, the V-SOA from in-basin biogenics is very small, and V-SOA is overwhelmingly from fossil carbon sources since it is dominated by aromatic precursors (see 3.1.3 below) and the main source of aromatic hydrocarbons in the Los Angeles basin is vehicle emissions (Borbon et al., 2013). For SI-SOA, two types of POA, and thus, primary P-S/IVOCs are included in this study. Since HOA is dominated by vehicle emissions, it is most likely composed of fossil carbon. On the other hand, CIOA will have a majority of modern carbon. In previous work we noted that 0 – 50% of the CIOA mass may be from non-cooking sources and, specifically, from vehicles (Hayes et al., 2013). Furthermore, recent results have shown that cooking emissions can form substantial amounts of SOA (El Haddad et al., 2012). If P-S/IVOCs emitted with HOA are 100% fossil carbon, P-S/IVOCs emitted with CIOA are 75(±25)% fossil, and both emission sources form SI-SOA with the same efficiency, then the corresponding amount of fossil SOA in the model would be 65(±9)%, 63(±12)%, 62(±12), and 78(±7)% for ROB, GRI, PYE, and ROB + 4xV, respectively. None of these predictions are significantly different from the ^{14}C measurements. An important caveat is that P-S/IVOCs from CIOA sources are modeled using the same parameters as P-S/IVOCs from HOA sources. It is possible that cooking and vehicle emissions do not exhibit the same SOA-forming properties, but it is not clear which would be a more potent SOA precursor as there are no parameterizations specific to cooking emissions available in the literature. Thus, the ROB, GRI, and PYE parameterizations are used for all P-S/IVOCs regardless of their source. It should also be noted that in Los Angeles gasoline contains nearly 10% ethanol made from corn and thus modern carbon (de Gouw et al., 2012), but it is thought that ethanol and its combustion products are not incorporated into aerosols (Lewis et al., 2006), although to our knowledge such measurements have not been performed for SOA particles.

As an extreme sensitivity study, the model variations were also run under the assumption that CIOA sources did not emit any P-S/IVOCs or, in the case of PYE variation, any SVOCs (Figure SI-5). The GRI, PYE, and ROB + 4xV variations reasonably reproduce the SV-OOA concentrations with some periods outside the measurement uncertainties. In contrast, the ROB

variation without cooking-related P-S/IVOCs predicts concentrations that are too low. Regardless of the parameterization, a strong urban source of non-fossil SOA precursors, such as cooking emissions, must be included to obtain agreement with the ^{14}C measurements; otherwise the modeled SOA is overwhelmingly fossil. Clearly, there are still large uncertainties in SOA formation from cooking emissions. Further studies are needed to constrain models and to identify potential additional urban sources of non-fossil SOA, although our results suggest that cooking emissions are a potentially important source of anthropogenic non-fossil SOA.

3.1.3. SOA concentration apportionment to precursor compounds

The diurnal cycles of V-SOA mass concentration produced from individual VOCs are shown in Figure 4A. Among the VOCs the five largest contributors to V-SOA are methyl-substituted aromatics such as xylenes, trimethylbenzenes, and toluene. When SOA concentrations peak, these compounds account for ~70% of the predicted V-SOA mass. In Figure 4B the precursor-specific model predictions are compared against results from a methodology developed by the U.S. EPA that apportions SOA to specific precursors using molecular tracers measured in ambient aerosol samples (Kleindienst et al., 2012). For methylbenzenes (i.e. aromatics containing one or more methyl substituents) the tracer molecule utilized is 2,3-dihydroxy-4-oxopentanoic acid, and for naphthalene, 1-methylnaphthalene, and 2-methylnaphthalene the tracer molecule is phthalic acid and the associated methyl-containing analogs. Several tracers are used for isoprene (Edney et al., 2005) and monoterpenes (Claeys et al., 2007; Szmigielski et al., 2007; Jaoui et al., 2005), and they are listed in Table SI-3 in the supporting information.

For the methylbenzenes, the model/tracer comparison is good, indicating consistency between model predictions and ambient measurements. The similarity further validates the model, although it is noted that if V-SOA 'aging' is eliminated from the model the model/tracer comparison improves further and the difference becomes less than 5%. We note that this comparison cannot constrain whether chamber yields have been reduced by vapor losses, since the same effect would have occurred when measuring the yields included in the model and when measuring the SOA/tracer ratio used for the tracer estimate. For the biogenic VOCs, isoprene and the monoterpenes, the tracer estimate indicates several-fold higher concentrations than predicted in the model. This difference is not surprising since the background SOA is thought to have a major contribution from isoprene and monoterpene oxidation in areas north of the Los Angeles Basin, and in the model BG-SOA from different VOCs is not resolved. In other words, the model results in Figure 4B represent only the in-basin biogenic SOA and are lower limits for total SOA from isoprene and monoterpenes. Moreover, the tracer estimates in Figure 4B are likely lower limits as well because Pasadena is influenced by background biogenic SOA and the tracers may be lost by subsequent heterogeneous oxidation as the background aerosol is transported to the measurement location (Hallquist et al., 2009). It therefore appears that the model/measurement comparison for the biogenic VOCs is qualitatively consistent given the known limitations of both approaches.

The last comparison in Figure 4B is for the naphthalenes. The tracer estimates are over an order-of-magnitude higher than the model predictions when using the SOA yields from the literature (which are ~20% for the conditions of our study) and the emission ratios determined from the regression analysis of nighttime measurements shown in Figure SI-3. The model is also run using the empirically adjusted emission ratios that better match the observed concentrations of the naphthalenes. One can observe that the model for this variation is still much lower than the tracer estimate. As an additional sensitivity study, we also run the model with the adjusted emissions and a yield of 150% that places all the oxidized mass in the C^*=1 μg m^{-3} volatility bin. This last variation represents an upper limit estimate of SOA from naphthalenes if all of their mass plus the added oxygen partitioned to the particle phase, which is much higher than laboratory observations. The tracer estimate, however, is still about a factor of two higher than the model. It is known that the tracer estimate is an upper limit, because the tracer compound, phthalic acid, may not be a unique tracer, and it potentially could be emitted from primary sources (Kleindienst et al., 2012). Thus, when considering this limitation it is concluded the model/measurement comparison is consistent. Utilizing the upper limit of the model results for naphthalene, including those from the parameterization with a purposefully high yield, it is apparent that naphthalene and its analogs account for less than 4% of the SOA mass. While previous work has suggested that PAHs are important precursors for SOA in the SoCAB (Hersey et al., 2011) these earlier findings were qualitative and based on the observation of phthalic acid in samples. The work presented here quantitatively demonstrates that PAHs are relatively unimportant compared to other precursors such as methylbenzenes. Lastly, we note that no suitable tracers for alkane oxidation have been identified yet, which prevents carrying out similar model/tracer comparisons with respect to the P-S/IVOCs, which are thought to be composed primarily of alkanes.

3.1.4. SOA concentration apportionment to gasoline versus diesel vehicles

In addition to apportioning the amount of SOA formed from individual compounds there is also considerable recent interest in the apportionment of SOA between diesel and gasoline vehicle emissions as well as other urban sources (Ensberg et al., 2014; Hayes et al., 2013; Bahreini et al., 2012; Gentner et al., 2012). The SOA model developed here can be used to address this important problem, and in Figure 5 the urban SOA mass calculated in the model is apportioned between diesel vehicles, gasoline vehicles, cooking sources, and in-basin biogenic emissions. The SOA mass is apportioned to each source using the following method, which can be described in five steps. First, the background is set to 2.1 μg m^{-3}. Second, the in-basin biogenic SOA is calculated as described in the methods section. Third, for the diesel contribution, since it is estimated that 70(±10)% of HOA is emitted from diesel vehicles (Hayes et al., 2013), it is assumed in the model that 70% of the P-S/IVOCs co-emitted with HOA are from diesel vehicles as well. While VOCs emissions from diesel vehicles are low (Warneke et al., 2012) in the Los Angeles Basin, VOCs have still been measured in diesel fuel. Specifically, using the measurements of Gentner et al. (2012) given in Tables S9 and S10 of that paper, the

percentage of each VOC included in our model emitted from diesel vehicles is calculated. The precursor-specific SOA concentrations, as shown in here in Figure 4, are then multiplied by these percentages to determine the fraction of V-SOA attributable to diesel emissions, which is 3%. It should be noted that for all the VOCs included here except 1,3-butadiene, styrene, and anthropogenic isoprene, the corresponding concentrations in gasoline and diesel fuel are published in Gentner et al. (2012). Fourth, the cooking contribution is calculated by assuming that 75% of the P-S/IVOCs co-emitted with CIOA are from cooking activities. This percentage is chosen since it lies halfway between 50 and 100%, which is the current constraint from measurements on the amount of CIOA from cooking sources as discussed above and in Hayes et al. (2013). Fifth, the gasoline fraction is taken to be the SOA formed from all the remaining VOCs as well as the remaining P-S/IVOCs.

As can be seen in Figure 5, for the urban SOA (i.e. excluding the background OA) diesel, gasoline, and cooking emissions all contribute substantially to SOA formation, with the sum of gasoline and cooking being much larger than diesel for all model variants. In contrast, the in-basin biogenic contribution is very small. The analogous results when the background is included are shown in the supporting information (Figure SI-6). The formation of SOA from diesel emissions accounts for 16 – 27% of the urban SOA in the model depending on the variant used. This result is very similar to the percentage reported in our previous work, 19(+17/-21)%, which was determined using measurements of OOA weekly cycles (Hayes et al., 2013). In addition, the diesel contribution in the model is consistent with PMF analysis of FTIR spectra of OA filter samples collected in Pasadena, in which, one SOA component exhibited relative peak intensities in the C-H stretching region that suggest qualitatively a contribution from diesel emissions (Guzman-Morales et al., 2014). The results of this work stand in contrast to those of Gentner et al. (2012) however, wherein the contribution of diesel and gasoline to vehicular SOA were estimated to be 70% and 30%, respectively.

Also shown in Figure 5 is a bar graph summarizing the result from each parameterization grouped by fossil and non-fossil sources as well as the fossil fraction of SV-OOA determined by Zotter et al. (2014), 71(±3)%. The results of the two studies are consistent, with cooking and in-basin biogenic SOA accounting for between 23 – 38% of the in-basin SOA mass in the models. These two sources represent the modern fraction in the box model.

The uncertainties shown in Figure 5 (in parentheses) are calculated by propagating the uncertainty in the amount of HOA from diesel sources, as well as the uncertainty in the amount of CIOA from cooking sources under the assumption that the P-S/IVOCs co-emitted with these primary aerosols have similar uncertainties. It is also noted that another source of uncertainty in the model is the selection of the GRI, ROB, PYE, and ROB + 4xV parameterizations. The model variant used has an important impact on the apportionment, but the greatest amount of urban SOA formed from diesel emission when considering all the uncertainties described in this paragraph is still only 31%.

3.1.5. Evolution of SOA concentration for 3 days

It is of high interest to explore the evolution of the different parameterizations discussed here at greater photochemical ages than those observed at the Pasadena site, since this behavior can lead to different results in regional and global modeling studies, and since similar combinations of parameterizations were found to over-predict regional SOA downwind of Mexico City (Dzepina et al., 2011). To explore this question, the evolution of SOA concentration was simulated for 3 days using each of the four major parameterizations (ROB, GRI, PYE, ROB + 4xV). The same simulation was carried out for the SIMPLE model and it is discussed below in Section 3.3. The results are shown in Figure 6, and in order to facilitate comparisons the SOA concentrations are normalized to the CO concentration, after subtracting the CO background (DeCarlo et al., 2010). The box model does not account for how dilution downwind of Los Angeles may increase SOA evaporation and thus the rate of oxidation via increased partitioning to the gas phase. However, this phenomenon would only lead to small changes in total model SOA, and that should not change the conclusions discussed in this section (Dzepina et al., 2011). Also shown in Figure 6 is the same ratio, SOA/ΔCO, determined previously from measurements at the Pasadena site (Hayes et al., 2013). At photochemical ages less than 0.25 days, GRI and ROB + 4xV perform the best (Table 4), which is consistent with the comparisons against the diurnal average of SOA since the diurnal photochemical age peaks at about 0.25 days (Figure 2A). However, for higher photochemical ages between 0.25 and 0.5 days the performance of ROB improves whereas that for GRI and ROB + 4xV worsens.

We also note that all of the parameterizations produce SOA/ΔCO ratios substantially larger (by factors of 2 or more) than those observed globally for aged air masses (i.e. photochemical ages greater than one day at an average OH concentration of 1.5×10^{6} molec cm^{-3}). For reference the range of OA/ΔCO ratios reported by de Gouw and Jimenez (2009) for aged urban SOA across multiple sites is indicated by the gray regions in Figure 6. This OA/ΔCO ratio includes both POA and SOA, but POA is a small contributor to OA/ΔCO for very aged air. These systematic over-predictions are important for regional and global models as they will lead to overestimation of urban SOA downwind of polluted regions. One possible explanation for the over-prediction is the lack of a fragmentation mechanism in the parameterizations, which would reduce the SOA mass by producing higher volatility products. Indeed, decreases in SOA concentration at high photochemical ages have been observed in flow-tube studies (e.g. Lambe et al., 2012).

3.1.6. Comparison of WRF-CMAQ versus measurements and box model

The comparison of the SOA predicted for Pasadena by the WRF-CMAQ model is shown in Figure 7A. Unlike the box model, the 3-D WRF-CMAQ model simulates the production and transport of SOA both within and outside the Los Angeles Basin. It is therefore most appropriate to compare the WRF-CMAQ model output with OOA (SV-OOA + LV-OOA) rather than just SV-OOA as is done for the box model that focused only on the urban area. The WRF-CMAQ SOA is well correlated with the measured OOA (R= 0.73), but the SOA mass concentration in

the model is ~25 times lower than the observed amount. This discrepancy is observed despite the fact that the VOCs show reasonable agreement (Supporting Information Figure SI-7, Panels A – C). The difference of a factor of 25 in the SOA concentrations is also observed consistently across different photochemical ages (Supporting Information Figure SI-7, Panel D). Furthermore, the performance of WRF-CMAQ is good for the inorganic aerosol species (Supporting Information Figures SI-8 and SI-9) as well as for elemental carbon and different meteorological parameters (Kelly et al., 2014; Baker et al., 2013). These comparisons indicate that while the model appears to be accurately simulating the transport to Pasadena and photochemical aging, the amount of SOA formed from urban precursors is greatly underestimated by WRF-CMAQ. Given the importance of P-S/IVOCs as SOA precursors in the box model, the lack of these species in WRF-CMAQ explains a substantial fraction of the difference between the models.

To further examine both WRF-CMAQ and the box model results, we modify the SOA module of the box model to be similar to the treatment of urban SOA in WRF-CMAQ as described by Carlton et al. (2010). First, for the box model P-S/IVOCs are not included, since these species are not in WRF-CMAQ. Second, the BG-SOA in the box model is adjusted to 0.1 μg m^{-3} so that the concentrations of SOA in the two models are similar in the early morning hours when the background dominates. Third, the box model uses a different approach for simulating V-SOA identical to that described by Dzepina et al. (2009). Briefly, instead of the VBS, an empirical 2-product parameterization wherein the oxidized products cannot undergo aging is used (Koo et al., 2003).

$$VOC + OH \rightarrow \alpha_1(SVOC_1) + \alpha_2(SVOC_2) \qquad (3)$$

The effective saturation concentration for each lumped product, *SVOC*, is then used to calculate the equilibrium partitioning between gas- and particle-phases as shown earlier in Equation 1.

The results of the comparison of WRF-CMAQ with the modified box model are shown in Figure 7B. With those modifications the results are very similar. This good agreement indicates that the differences between the default box model and WRF-CMAQ are not due to differences in transport or another variable, but rather to the intrinsic differences in the SOA modules. In addition, the comparison between the two models suggests that 3-D air quality models need to include either SOA from P-S/IVOCs, additional precursor sources, and/or increased V-SOA yields to accurately predict SOA concentrations in the Los Angeles Basin and other urban areas.

3.2. Comparison of predicted and measured SOA oxygen content

The diurnal cycle of O:C of total OA is shown in Figure 8, along with the estimated ±30% uncertainty of the O:C determination (2008; Aiken et al., 2007). A recent re-evaluation of the AMS elemental analysis has found an underestimation of oxygen content for multi-functional oxidized organics (Canagaratna et al., 2014). Thus, the updated calibration factors have been

used in the work here, and they increase the measured O:C and H:C by factors of 1.28 and 1.1, respectively. The model predictions of O:C are shown for both the ROB and GRI parameterizations of SI-SOA. The measured O:C ratio is similar or higher than the models, and exhibits small changes during the day due to the presence of BG-SOA, which is a large portion of the total OA mass. The minimum after noon in the measured O:C is due to the arrival of POA above Pasadena as well as the production of fresh SOA. The second minimum in the evening is due to emissions of CIOA, which has relatively low oxygen content.

When the model is run with the ROB parameterization for O:C evolution in SOA the model diurnal cycle is generally lower than the field data. Similar to the comparison of mass concentration, the GRI parameterization better reproduces the O:C observations. As a control the model is also run without SI-SOA, which, interestingly, also does an excellent job of reproducing the observations. Two conclusions can be drawn from the results shown in Figure 8. First, the SI-SOA in the ROB parameterization appears to be not sufficiently oxidized, which drives down the predicted O:C ratio, and, in general, SOA production and oxidation in Pasadena is very rapid and is therefore best described by the GRI parameterization. Second, both SI-SOA from the GRI parameterization and V-SOA have an O:C of ~ 0.45, which is not very different from the weighted mean of HOA, CIOA, and LV-OOA (O:C ~ 0.6), and, as a result, the O:C is relatively constant for the different times of day. This consideration also explains why O:C does not change substantially when the GRI parameterized SI-SOA is included or excluded in the model.

3.3. A simple parameterization for SOA formation in polluted urban regions.

While medium-complexity parameterizations of SOA formation and evolution such as those used above represent some important details of SOA chemistry and properties, there is a need for very computationally inexpensive SOA parameterizations that still retain good accuracy for use in regional, global, and climate models. Such a parameterization was recently reported by Hodzic and Jimenez (2011), and was designed to predict properties of urban SOA in global and climate modeling studies (referred to as the "SIMPLE" parameterization hereinafter). The model represents SOA precursors as a single surrogate lumped species, termed here 'VOC*', which is emitted proportionally to anthropogenic CO. The model converts VOC* to SOA by reaction with OH with a specified rate constant. The SOA formed in the SIMPLE model is non-volatile and does not partition to the gas-phase, consistent with the low volatility observed for aged SOA in field studies (e.g., Cappa and Jimenez, 2010).

We replaced the SOA parameterizations discussed above with the SIMPLE parameterization just described, and ran the box model for a large number of possible parameter value combinations (i.e. emission ratio of VOC*/CO and OH rate constant). Figure 9A shows the difference between model and measurement over that parameter space. The diurnal cycle predicted by the SIMPLE parameterization with the optimum parameters is shown in Figure 9B. The SIMPLE model with the optimized parameters performs comparably to the more complex parameterizations used in this work. Interestingly, the optimal model parameters for Mexico City

and Pasadena are very similar, which suggests the SIMPLE model can be applied to other polluted urban regions as well. In addition, the optimal parameters for Pasadena (and Mexico City) are consistent with the OA/ΔCO ratios observed for highly aged air masses as summarized by de Gouw and Jimenez (2009). However, it should be noted that a range of SIMPLE parameter combinations still remains in which the different combinations perform similarly in the model/measurement comparison, and this range is indicated by the dashed box in Figure 9. This lack of a precise constraint is due to the limited range of photochemical ages observed at most stationary field sites. However, the SOA formed at high ages by the optimal SIMPLE parameterization is consistent with the SOA concentrations observed at high ages in polluted air (Figure 6). Nevertheless, additional work should be carried out to verify the optimal SIMPLE model parameters including analysis of data for a broad range of ages, e.g., by utilizing results from ambient air processed by oxidation flow reactors (Ortega et al., 2013).

Hodzic and Jimenez (2011) also proposed an approach for predicting the oxygen content of OA that utilized the equation O:C = 1 – 0.6exp(-*A*/1.5), where *A* is the photochemical age in days. (Note: the photochemical age was calculated using a reference OH concentration of 1.5×10^{6} molec cm^{-3}.) As shown in Figure 10, this parameterization compares well with the O:C ratio from measurements. However, the parameterization of Hodzic and Jimenez does not take into account the new AMS O:C calibrations factors, as described in the preceding section. In order to account for this change, the equation proposed by Hodzic and Jimenez must be multiplied by a factor of 1.28. Thus, the updated parameterization is O:C = 1.28(1 – 0.6exp(-*A*/1.5)), and the corresponding O:C values are shown in Figure 10. The updated simple parameterization also exhibits good agreement with measurements. (Note: The O:C predicted by the updated model does not increase by a factor 1.28 relative to the original version because the SOA from the Hodzic and Jimenez parameterization is mixed with HOA, CIOA, and BG-SOA to determine the total OA O:C shown in Figure 10.).

3.4 Update of the US and Global Urban SOA budgets

As shown in Figure 6, the SIMPLE parameterization asymptotically approaches a SOA/ΔCO value of 80 μg m^{-3} ppm^{-1}, which can be used to estimate an urban SOA budget. For the U.S., the annual urban CO emissions reported in the 2011 National Emissions Inventory are 44 Tg (EPA, 2013), which when multiplied by SOA/ΔCO gives an urban SOA source of 3.1 Tg. For reference, from the same database the national biogenic VOCs emissions are 37 Tg. Then using an approximate yield of 10%, the biogenic VOCs would represent a SOA source of 3.7 Tg. While there are several major uncertainties in this analysis – the accuracy of the SIMPLE model at greater photochemical ages, yields for biogenic VOCs, etc. – it is evident that the amount of urban SOA is not negligible compared to the amount of biogenic SOA in the U.S. The same estimate can be performed for global urban SOA, since similar ratios of SOA/ΔCO have been observed in other areas such as downwind of Mexico City and China (Hu et al., 2013; DeCarlo et al., 2010). Using the EDGAR v4.2 inventory of 432 Tg yr^{-1} of urban/industrial CO for 2008 (JRC, 2011), we estimate a global pollution SOA source of 26 Tg yr^{-1}, or about 17% of the

estimated global SOA source of 150 Tg yr^{-1} (Heald et al., 2011; Spracklen et al., 2011; Heald et al., 2010; Hallquist et al., 2009). We note that 1/3 of that SOA would be non-fossil, if a similar cooking fraction is observed globally as in this study, which is expected given the identification of similar fractions of cooking POA in many field studies globally (Mohr et al., 2011; Sun et al., 2011; Wang et al., 2009).

4. Conclusions

SOA in Pasadena during CalNex has been modeled using three different methods: (1) a box model, (2) a 3-D dimension model, namely, WRF-CMAQ, and (3) a simple two-parameter model. Model/measurement comparisons clearly indicate that SOA formed from P-S/IVOCs, or a similar source, must be included in the models to accurately predict SOA concentrations in Pasadena. In other words, SOA from VOC oxidation is not sufficient to explain the observed concentrations, even when the highest SOA yields are used. Specifically, the parameterizations utilized were the Tsimpidi et al. (2010) parameterization with aging or a modified version of that parameterization in which the SOA yields for aromatic VOCs were multiplied by four as recently suggested by Zhang et al. (2014).

Three parameterizations for SOA formation from P-S/IVOCs were tested. It was found that the parameterization reported by Grieshop et al. (2009) best predicts both SOA concentration and SOA oxygen content. In contrast, the parameterization of Robinson et al. (2007) predicts too little SOA and too low oxygen content. These results contrast earlier modeling studies of Mexico City that showed the Robinson parameterization performed better when compared against the measured SOA concentration. The reason for the difference is not clear although it may be attributable to a different mixture of P-S/IVOCs at the two locations. Both the Mexico City and Pasadena studies indicate that the Grieshop parameterization more accurately predicts SOA oxygen content. Additionally, we tested the parameterization proposed in Pye and Seinfeld (2010) for the formation of SOA from P-S/IVOCs, which produces similar results but tends to over predict SOA concentrations especially at nighttime for this case study. The relative importance of VOCs and P-S/IVOCs as contributors to urban SOA over different time and length scales remains unclear. All the parameterizations over-predict urban SOA at photochemical ages larger than one day compared to field observations, which has implications for their use in regional and global models.

This work represents the first chemically explicit evaluation of WRF-CMAQ SOA mass predictions in the Western U.S. or California. This model provides excellent predictions of secondary inorganic particles species but underestimates the observed SOA mass by a factor of about 25. The discrepancy is likely attributable to the VOC-only parameterization used that has relatively low yields and does not include SOA from P-S/IVOCs or a similar source.

SOA source apportionment was also carried out using the box model results. Among the VOCs, the precursor compounds that contribute the most SOA mass are all methylbenzenes. In contrast, PAHs (i.e. naphthalene, 1-methylnaphthalene, and 2-methylnaphthalene) are relatively minor precursors and contribute less than 4% of the SOA mass. In addition, the amount of urban

SOA from diesel vehicles, gasoline vehicles, and cooking-related emissions is estimated to be 16 – 27%, 35 – 61%, and 19 – 35%, respectively. A significant amount of SOA appears to be formed outside the Los Angeles Basin and transported to the Pasadena site. The percentage estimated from diesel in the model is in agreement with our previous study that estimated the diesel contribution to be 0 – 36% by analyzing the weekly cycle of OOA concentrations (Hayes et al., 2013). The fraction of fossil and non-fossil SOA from the different models is generally consistent with the measurements. Importantly a large source of urban non-fossil SOA most likely due to cooking is identified, while biogenic SOA formed from urban emissions makes a small contribution.

The final portion of this work adapts the SIMPLE two parameter model of Hodzic and Jimenez (2011) to predict SOA properties for Pasadena. The simple model successfully predicts SOA concentration and oxygen content with accuracy similar to the more complex box model. Furthermore, the optimal parameters for the SIMPLE model are very similar in both Mexico City and Pasadena, which indicates that this computationally inexpensive approach may be useful for predicting pollution SOA in global and climate models. Pollution SOA is estimated to account for 17% of global SOA, and we note that ~1/3 of urban SOA may be non-fossil mainly due to the impact of cooking sources.

5. Acknowledgements

This work was partially supported by CARB 08-319 and CARB 11-305, US DOE (BER, ASR program) DE-SC0006035, DE-SC0006711, and DE-SC0011105, NSF AGS-1243354 and AGS-1360834, and NOAA NA13OAR4310063. PLH is also grateful for a fellowship from the CIRES Visiting Fellows Program. The authors thank Chris J. Hennigan (UMBC) and Allen L. Robinson (CMU) for providing the naphthalene and methylnaphthalene data. We also thank John S. Holloway (NOAA) for providing CO data, as well as Stuart A. McKeen (NOAA) for helpful discussions. RA is supported by the US Weather Research Program within NOAA/OAR Office of Weather and Air Quality. The US Environmental Protection Agency through its Office of Research and Development collaborated in the research described here. The manuscript has been subjected to external peer review and has not been cleared for publication. Mention of trade names or commercial products does not constitute endorsement or recommendation for use.

6. Figure Captions

Table 1. Definitions of acronyms frequently used in this article.

Table 2. Summary of the SOA models and their major variants used in this work.

Table 3. Measurements acquired at the Pasadena ground site during CalNex and used in this study.

Table 4. Slope of SOA/ΔCO as reported by Hayes et al. (2013), and as predicted in the four major box model variations. For the box model, the slopes are obtained by performing a linear regression analysis on the data shown in Figure 6.

Figure 1. Schematic of the major SOA parameterizations used in the box model. The different regions of the volatility scale are indicated on the top axis: low-volatility organic compounds (LVOCs), semi-volatile organic compounds (SVOCs), intermediate volatility organic compounds (IVOCs), and volatile organic compounds (VOCs). The fraction in the particle phase, F_p (top panel), increases with decreasing volatility (i.e. C^*) according to equation 1. The parameterization of Tsimpidi et al. (2010) distributes the VOC oxidation products into four volatility bins, and subsequent oxidation reactions are allowed as indicated by the curved arrows. The two parameterizations for P-S/IVOC oxidation from Robinson et al. (2007) and Grieshop et al. (2009) are illustrated as well. Lastly, the parameterization of Pye and Seinfeld (2010) is shown in which SVOCs are treated as four lumped species (pink), and IVOCs are treated using the yields and volatility distribution for naphthalene oxidation (yellow). For clarity the arrows indicating IVOC aging are not shown.

Figure 2. (A) Average diurnal cycle of CO (red) and photochemical age (blue) for the Pasadena ground site during CalNex. Note: A background of 105 ppbv has been subtracted from the CO concentration. **(B)** Average diurnal cycle of the five OA components identified by PMF analysis, as well as the background OA calculated from WRF-Chem. The five components are semi-volatile oxygenated organic aerosol (SV-OOA), cooking-influenced organic aerosol (CIOA), hydrocarbon-like organic aerosol (HOA), local organic aerosol (LOA), and low volatility organic aerosol (LV-OOA).

Figure 3. Model/measurement comparisons for urban SOA mass concentration plotted by time of day. The model results are shown for the Robinson et al. (2007) parameterization **(ROB)**, the Grieshop et al. (2009) parameterization **(GRI)**, the Pye and Seinfeld (2010) parameterization **(PYE)**, and for a modified parameterization in which the yields for the aromatic VOCs have been increased by a factor of 4 while aging is not allowed **(ROB + 4xV)**. In all panels the SV-OOA determined from measurements at the Pasadena ground site is shown (black solid lines). The uncertainty for the AMS measurement used to determine the SV-OOA concentration is indicated by the dashed lines (Middlebrook et al., 2012). Also shown are the model

concentrations for SI-SOA, as well as V-SOA from anthropogenic VOCs and biogenic VOCs. For the PYE parameterization SOA concentrations from primary SVOCs and primary IVOCs are shown separately.

Figure 4. (A) Predicted SOA mass from important precursor VOCs. For clarity only the five largest contributors to the SOA mass are shown. Note that SI-SOA from P-S/IVOCs is not included in this panel. **(B)** Campaign average concentrations of SOA from specific precursors as determined in the box model as well as by the U.S. EPA tracer method (Kleindienst et al., 2012). Comparisons are shown for methylbenzenes, naphthalenes, isoprene, and monoterpenes. For the naphthalenes the bar for "adjusted emissions" indicates the model variation where the naphthalene emissions are increased in order to match the measured concentrations in Pasadena as shown in Figure SI-3. The adjusted emissions are also used for the variation with a yield of 1.5 at C*=1. Note: The GRI parameterization is used to predict the SI-SOA for both of these panels.

Figure 5. The estimated fractional contribution to SOA mass concentration from gasoline vehicles, diesel vehicles, cooking emissions, and in-basin biogenic emissions. The results for the four model variations are displayed as pie charts as well as a bar chart. The bar chart also shows the percentage of SOA that is from fossil or modern sources as determined by Zotter et al. (2014). The modern sources are indicated by hollow bars and fossil sources are indicated by solid bars.

Figure 6. SOA concentration predicted by the GRI, ROB, PYE, and ROB + 4xV parameterizations for up to 3 days of photochemical aging at a reference OH concentration of 1.5×10^{6} molec cm^{-3}. Also shown in the four panels is the same result for the SIMPLE model using the optimized parameters. Note that the SOA concentrations has been normalized to the background subtracted CO concentration to account for changes in emission strengths, and the processed data are identified by the symbol SOA/ΔCO. In addition, the SOA/ΔCO data determined for the Pasadena site from the measurements of Hayes et al. (2013) are shown (solid black line). The OA/ΔCO ratio reported by de Gouw and Jimenez (2009) is also indicated (gray box) to serve as an estimate of OOA/ΔCO in highly aged air masses. For clarity, the uncertainty in the SOA determined from measurements (±30%) is not shown.

Figure 7. (A) Scatter plot of SOA predicted by the WRF-CMAQ model versus the OOA determined from measurements at the Pasadena ground site. Also shown in this panel is an ODR linear regression analysis of the data (black line) with the y-intercept fixed to zero. **(B)** SOA diurnal cycles from the WRF-CMAQ and box model. The box model was run using an empirical two product parameterization (i.e., Model Variant 5 in Table 2) wherein the oxidized products cannot undergo aging (Dzepina et al., 2009). See text for further details.

Figure 8. Model/measurement comparison for O:C of OA versus time of day. The left panel contains the results when using the Robinson et al. (2007) parameterization and the right panel

when using Grieshop et al. (2009) parameterization. In both panels the O:C of OA measured at the Pasadena ground site is shown (black line) along with the O:C uncertainty (gray shading). Shown in both panels also is the model O:C when including only the SOA from VOCs (blue line), and the O:C from the models variants that include SOA from both VOCs and P-S/IVOCs (pink line).

Figure 9. (Left) Image plot of the root mean square error between the SIMPLE urban SOA parameterization concentration and the measured SV-OOA as a function of both the lumped precursor emission ratio and the oxidation rate constant. The gray and red stars indicate the parameter pairs that result in the minimum errors for Pasadena (this study) and Mexico City (Hodzic and Jimenez, 2011). The dashed box approximately indicates the range of possible optimal parameter combinations. For reference an emission ratio of 80 $\mu g\ m^{-3}\ ppmv^{-1}$ equals 0.069 $g\ g^{-1}$. **(Right)** Diurnal cycle of SV-OOA (black solid line) with corresponding uncertainty (grey dashed lines). The diurnal cycle of SOA predicted by the SIMPLE model is shown as well (green).

Figure 10. Model/measurement comparison of O:C of OA versus time of day for the SIMPLE urban SOA parameterization. The original parameterization proposed by Hodzic and Jimenez (2011) is O:C = $1 - 0.6\exp(-A/1.5)$, where A is the photochemical age (pink line). The updated SIMPLE parameterization is O:C = $1.28(1 - 0.6\exp(-A/1.5))$, which accounts for the updated AMS O:C calibration factors.

7. References

Ahmadov, R., McKeen, S.A., Robinson, A.L., Bahreini, R., Middlebrook, A.M., de Gouw, J.A., Meagher, J., Hsie, E.Y., Edgerton, E., Shaw, S. and Trainer, M. (2012) A volatility basis set model for summertime secondary organic aerosols over the eastern United States in 2006. J. Geophys. Res.-Atmos. 117, D06301.

Aiken, A.C., DeCarlo, P.F. and Jimenez, J.L. (2007) Elemental analysis of organic species with electron ionization high-resolution mass spectrometry. Anal. Chem. 79, 8350-8358.

Aiken, A.C., Decarlo, P.F., Kroll, J.H., Worsnop, D.R., Huffman, J.A., Docherty, K.S., Ulbrich, I.M., Mohr, C., Kimmel, J.R., Sueper, D., Sun, Y., Zhang, Q., Trimborn, A., Northway, M., Ziemann, P.J., Canagaratna, M.R., Onasch, T.B., Alfarra, M.R., Prevot, A.S.H., Dommen, J., Duplissy, J., Metzger, A., Baltensperger, U. and Jimenez, J.L. (2008) O/C and OM/OC ratios of primary, secondary, and ambient organic aerosols with high-resolution time-of-flight aerosol mass spectrometry. Environ. Sci. Technol. 42, 4478-4485.

Atkinson, R. and Arey, J. (2003) Atmospheric degradation of volatile organic compounds. Chem. Rev. 103, 4605-4638.

Bahreini, R., Middlebrook, A.M., de Gouw, J.A., Warneke, C., Trainer, M., Brock, C.A., Stark, H., Brown, S.S., Dube, W.P., Gilman, J.B., Hall, K., Holloway, J.S., Kuster, W.C., Perring, A.E., Prevot, A.S.H., Schwarz, J.P., Spackman, J.R., Szidat, S., Wagner, N.L., Weber, R.J., Zotter, P. and Parrish, D.D. (2012) Gasoline emissions dominate over diesel in formation of secondary organic aerosol mass. Geophys. Res. Lett. 39, L06805.

Baker, K.R., Misenis, C., Obland, M.D., Ferrare, R.A., Scarino, A.J. and Kelly, J.T. (2013) Evaluation of surface and upper air fine scale WRF meteorological modeling of the May and June 2010 CalNex period in California. Atmos. Environ. 80, 299-309.

Bertram, A.K., Martin, S.T., Hanna, S.J., Smith, M.L., Bodsworth, A., Chen, Q., Kuwata, M., Liu, A., You, Y. and Zorn, S.R. (2011) Predicting the relative humidities of liquid-liquid phase separation, efflorescence, and deliquescence of mixed particles of ammonium sulfate, organic material, and water using the organic-to-sulfate mass ratio of the particle and the oxygen-to-carbon elemental ratio of the organic component. Atmos. Chem. Phys. 11, 10995-11006.

Borbon, A., Gilman, J.B., Kuster, W.C., Grand, N., Chevaillier, S., Colomb, A., Dolgorouky, C., Gros, V., Lopez, M., Sarda-Esteve, R., Holloway, J., Stutz, J., Petetin, H., McKeen, S., Beekmann, M., Warneke, C., Parrish, D.D. and de Gouw, J.A. (2013) Emission ratios of anthropogenic volatile organic compounds in northern mid-latitude megacities: Observations versus emission inventories in Los Angeles and Paris. J. Geophys. Res.-Atmos. 118, 2041-2057.

Canagaratna, M.R., Jimenez, J.L., Kroll, J., Chen, Q., Kessler, S., Massoli, P., Hildebrandt, L., Fortner, E., Williams, L., Wilson, K., Surratt, J., Donahue, N., Jayne, J.T. and Worsnop, D.R. (2014) Elemental Ratio Measurements of Organic Compounds using Aerosol Mass Spectrometry: Characterization, Improved Calibration, and Implications. Atmos. Chem. Phys. Discuss. Submitted.

Cappa, C.D. and Jimenez, J.L. (2010) Quantitative estimates of the volatility of ambient organic aerosol. Atmos. Chem. Phys. 10, 5409-5424.

Cappa, C.D., Onasch, T.B., Massoli, P., Worsnop, D.R., Bates, T.S., Cross, E.S., Davidovits, P., Hakala, J., Hayden, K.L., Jobson, B.T., Kolesar, K.R., Lack, D.A., Lerner, B.M., Li,

S.M., Mellon, D., Nuaaman, I., Olfert, J.S., Petaja, T., Quinn, P.K., Song, C., Subramanian, R., Williams, E.J. and Zaveri, R.A. (2012) Radiative Absorption Enhancements Due to the Mixing State of Atmospheric Black Carbon. Science 337, 1078-1081.

Cappa, C.D. and Wilson, K.R. (2011) Evolution of organic aerosol mass spectra upon heating: implications for OA phase and partitioning behavior. Atmos. Chem. Phys. 11, 1895-1911.

Carlton, A.G. and Baker, K.R. (2011) Photochemical Modeling of the Ozark Isoprene Volcano: MEGAN, BEIS, and Their Impacts on Air Quality Predictions. Environ. Sci. Technol. 45, 4438-4445.

Carlton, A.G., Bhave, P.V., Napelenok, S.L., Edney, E.D., Sarwar, G., Pinder, R.W., Pouliot, G.A. and Houyoux, M. (2010) Model Representation of Secondary Organic Aerosol in CMAQv4.7. Environ. Sci. Technol. 44, 8553-8560.

Carlton, A.G., Turpin, B.J., Altieri, K.E., Seitzinger, S.P., Mathur, R., Roselle, S.J. and Weber, R.J. (2008) CMAQ model performance enhanced when in-cloud SOA is included: comparisons of OC predictions with measurements. Environ. Sci. Technol. 42, 8798-8802.

Carter, W.P.L. (2010) Development of the SAPRC-07 chemical mechanism. Atmos. Environ. 44, 5324-5335.

Chan, A.W.H., Kautzman, K.E., Chhabra, P.S., Surratt, J.D., Chan, M.N., Crounse, J.D., Kürten, A., Wennberg, P.O., Flagan, R.C. and Seinfeld, J.H. (2009) Secondary organic aerosol formation from photooxidation of naphthalene and alkylnaphthalenes: implications for oxidation of intermediate volatility organic compounds (IVOCs). Atmos. Chem. Phys. 9, 3049-3060.

Chen, Q., Farmer, D.K., Schneider, J., Zorn, S.R., Heald, C.L., Karl, T.G., Guenther, A., Allan, J.D., Robinson, N., Coe, H., Kimmel, J.R., Pauliquevis, T., Borrmann, S., Poschl, U., Andreae, M.O., Artaxo, P., Jimenez, J.L. and Martin, S.T. (2009) Mass spectral characterization of submicron biogenic organic particles in the Amazon Basin. Geophys. Res. Lett. 36, L20806.

Claeys, M., Szmigielski, R., Kourtchev, I., Van der Veken, P., Vermeylen, R., Maenhaut, W., Jaoui, M., Kleindienst, T.E., Lewandowski, M., Offenberg, J.H. and Edney, E.O. (2007) Hydroxydicarboxylic Acids: Markers for Secondary Organic Aerosol from the Photooxidation of α-Pinene. Environ. Sci. Technol. 41, 1628-1634.

de Gouw, J. and Jimenez, J.L. (2009) Organic Aerosols in the Earth's Atmosphere. Environ. Sci. Technol. 43, 7614-7618.

de Gouw, J.A., Gilman, J.B., Borbon, A., Warneke, C., Kuster, W.C., Goldan, P.D., Holloway, J.S., Peischl, J., Ryerson, T.B., Parrish, D.D., Gentner, D.R., Goldstein, A.H. and Harley, R.A. (2012) Increasing atmospheric burden of ethanol in the United States. Geophys. Res. Lett. 39, L15803.

DeCarlo, P.F., Ulbrich, I.M., Crounse, J., de Foy, B., Dunlea, E.J., Aiken, A.C., Knapp, D., Weinheimer, A.J., Campos, T., Wennberg, P.O. and Jimenez, J.L. (2010) Investigation of the sources and processing of organic aerosol over the Central Mexican Plateau from aircraft measurements during MILAGRO. Atmos. Chem. Phys. 10, 5257-5280.

Docherty, K.S., Stone, E.A., Ulbrich, I.M., DeCarlo, P.F., Snyder, D.C., Schauer, J.J., Peltier, R.E., Weber, R.J., Murphy, S.M., Seinfeld, J.H., Grover, B.D., Eatough, D.J. and Jimenez, J.L. (2008) Apportionment of Primary and Secondary Organic Aerosols in

Southern California during the 2005 Study of Organic Aerosols in Riverside (SOAR-1). Environ. Sci. Technol. 42, 7655-7662.

Dockery, D.W. and Pope, C.A. (1994) Acute respiratory effects of particulate air-pollution. Annu. Rev. Publ. Health 15, 107-132.

Donahue, N.M., Chuang, W., Epstein, S.A., Kroll, J.H., Worsnop, D.R., Robinson, A.L., Adams, P.J. and Pandis, S.N. (2013) Why do organic aerosols exist? Understanding aerosol lifetimes using the two-dimensional volatility basis set. Environmental Chemistry 10, 151-157.

Donahue, N.M., Robinson, A.L., Stanier, C.O. and Pandis, S.N. (2006) Coupled partitioning, dilution, and chemical aging of semivolatile organics. Environ. Sci. Technol. 40, 2635-2643.

Dzepina, K., Cappa, C.D., Volkamer, R.M., Madronich, S., DeCarlo, P.F., Zaveri, R.A. and Jimenez, J.L. (2011) Modeling the Multiday Evolution and Aging of Secondary Organic Aerosol During MILAGRO 2006. Environ. Sci. Technol. 45, 3496-3503.

Dzepina, K., Volkamer, R.M., Madronich, S., Tulet, P., Ulbrich, I.M., Zhang, Q., Cappa, C.D., Ziemann, P.J. and Jimenez, J.L. (2009) Evaluation of recently-proposed secondary organic aerosol models for a case study in Mexico City. Atmos. Chem. Phys. 9, 5681-5709.

Edney, E.O., Kleindienst, T.E., Jaoui, M., Lewandowski, M., Offenberg, J.H., Wang, W. and Claeys, M. (2005) Formation of 2-methyl tetrols and 2-methylglyceric acid in secondary organic aerosol from laboratory irradiated isoprene/NOX/SO2/air mixtures and their detection in ambient PM2.5 samples collected in the eastern United States. Atmos. Environ. 39, 5281-5289.

El Haddad, I., Platt, S., Slowik, J.G., Mohr, C., Crippa, M., Temime-Roussel, B., Detournay, A., Marchand, N., Baltensperger, U. and Prevot, A.S.H. (2012) *Contributions of Cooking Emissions to Primary and Secondary Organic Aerosol in Urban Atmospheres*, American Association for Aerosol Research 31st Annual Conference, Minneapolis, Minnesota http://aaarabstracts.com/2012/AbstractBook.pdf

Ensberg, J.J., Hayes, P.L., Jimenez, J.L., Gilman, J.B., Kuster, W.C., de Gouw, J.A., Holloway, J.S. and Seinfeld, J.H. (2014) Emission factor ratios, SOA mass yields, and the impact of vehicular emissions on SOA formation. Atmos. Chem. Phys. 14, 2383-2397.

EPA (2013) *National Emissions Inventory*. Environmental Protection Agency http://www.epa.gov/ttn/chief/net/2011inventory.html

Ervens, B. and Volkamer, R. (2010) Glyoxal processing by aerosol multiphase chemistry: towards a kinetic modeling framework of secondary organic aerosol formation in aqueous particles. Atmos. Chem. Phys. 10, 8219-8244.

Fountoukis, C. and Nenes, A. (2007) ISORROPIA II: a computationally efficient thermodynamic equilibrium model for K+-Ca2+-Mg2+-Nh(4)(+)-Na+-SO42--NO3--Cl--H2O aerosols. Atmos. Chem. Phys. 7, 4639-4659.

Gentner, D.R., Isaacman, G., Worton, D.R., Chan, A.W.H., Dallmann, T.R., Davis, L., Liu, S., Day, D.A., Russell, L.M., Wilson, K.R., Weber, R., Guha, A., Harley, R.A. and Goldstein, A.H. (2012) Elucidating secondary organic aerosol from diesel and gasoline vehicles through detailed characterization of organic carbon emissions. Proc. Natl. Acad. Sci. U. S. A. 109, 18318-18323.

Grieshop, A.P., Logue, J.M., Donahue, N.M. and Robinson, A.L. (2009) Laboratory investigation of photochemical oxidation of organic aerosol from wood fires 1:

measurement and simulation of organic aerosol evolution. Atmos. Chem. Phys. 9, 1263-1277.

Griffin, R.J., Chen, J.J., Carmody, K., Vutukuru, S. and Dabdub, D. (2007) Contribution of gas phase oxidation of volatile organic compounds to atmospheric carbon monoxide levels in two areas of the United States. J. Geophys. Res.-Atmos. 112, D10S17.

Guzman-Morales, J., Frossard, A.A., Corrigan, A.L., Russell, L.M., Liu, S., Takahama, S., Taylor, J.W., Allan, J., Coe, H., Zhao, Y. and Goldstein, A.H. (2014) Estimated contributions of primary and secondary organic aerosol from fossil fuel combustion during the CalNex and Cal-Mex campaigns. Atmos. Environ. 88, 330-340.

Hallquist, M., Wenger, J.C., Baltensperger, U., Rudich, Y., Simpson, D., Claeys, M., Dommen, J., Donahue, N.M., George, C., Goldstein, A.H., Hamilton, J.F., Herrmann, H., Hoffmann, T., Iinuma, Y., Jang, M., Jenkin, M.E., Jimenez, J.L., Kiendler-Scharr, A., Maenhaut, W., McFiggans, G., Mentel, T.F., Monod, A., Prevot, A.S.H., Seinfeld, J.H., Surratt, J.D., Szmigielski, R. and Wildt, J. (2009) The formation, properties and impact of secondary organic aerosol: current and emerging issues. Atmos. Chem. Phys. 9, 5155-5236.

Hayes, P.L., Ortega, A.M., Cubison, M.J., Froyd, K.D., Zhao, Y., Cliff, S.S., Hu, W.W., Toohey, D.W., Flynn, J.H., Lefer, B.L., Grossberg, N., Alvarez, S., Rappenglück, B., Taylor, J.W., Allan, J.D., Holloway, J.S., Gilman, J.B., Kuster, W.C., de Gouw, J.A., Massoli, P., Zhang, X., Liu, J., Weber, R.J., Corrigan, A.L., Russell, L.M., Isaacman, G., Worton, D.R., Kreisberg, N.M., Goldstein, A.H., Thalman, R., Waxman, E.M., Volkamer, R., Lin, Y.H., Surratt, J.D., Kleindienst, T.E., Offenberg, J.H., Dusanter, S., Griffith, S., Stevens, P.S., Brioude, J., Angevine, W.M. and Jimenez, J.L. (2013) Organic aerosol composition and sources in Pasadena, California during the 2010 CalNex campaign. J. Geophys. Res.-Atmos., 9233-9257.

Heald, C.L., Coe, H., Jimenez, J.L., Weber, R.J., Bahreini, R., Middlebrook, A.M., Russell, L.M., Jolleys, M., Fu, T.M., Allan, J.D., Bower, K.N., Capes, G., Crosier, J., Morgan, W.T., Robinson, N.H., Williams, P.I., Cubison, M.J., DeCarlo, P.F. and Dunlea, E.J. (2011) Exploring the vertical profile of atmospheric organic aerosol: comparing 17 aircraft field campaigns with a global model. Atmos. Chem. Phys. 11, 12673-12696.

Heald, C.L., Ridley, D.A., Kreidenweis, S.M. and Drury, E.E. (2010) Satellite observations cap the atmospheric organic aerosol budget. Geophys. Res. Lett. 37, L24808.

Hersey, S.P., Craven, J.S., Schilling, K.A., Metcalf, A.R., Sorooshian, A., Chan, M.N., Flagan, R.C. and Seinfeld, J.H. (2011) The Pasadena Aerosol Characterization Observatory (PACO): chemical and physical analysis of the Western Los Angeles basin aerosol. Atmos. Chem. Phys. 11, 7417-7443.

Hodzic, A. and Jimenez, J.L. (2011) Modeling anthropogenically-controled secondary organic aerosols in a megacity: a simplified framework for global and climate models. Geosci. Model Dev. 4, 901-917.

Hodzic, A., Jimenez, J.L., Madronich, S., Aiken, A.C., Bessagnet, B., Curci, G., Fast, J., Lamarque, J.F., Onasch, T.B., Roux, G., Schauer, J.J., Stone, E.A. and Ulbrich, I.M. (2009) Modeling organic aerosols during MILAGRO: importance of biogenic secondary organic aerosols. Atmos. Chem. Phys. 9, 6949-6981.

Hodzic, A., Jimenez, J.L., Madronich, S., Canagaratna, M.R., DeCarlo, P.F., Kleinman, L. and Fast, J. (2010a) Modeling organic aerosols in a megacity: potential contribution of semi-

volatile and intermediate volatility primary organic compounds to secondary organic aerosol formation. Atmos. Chem. Phys. 10, 5491-5514.

Hodzic, A., Jimenez, J.L., Prevot, A.S.H., Szidat, S., Fast, J.D. and Madronich, S. (2010b) Can 3-D models explain the observed fractions of fossil and non-fossil carbon in and near Mexico City? Atmos. Chem. Phys. 10, 10997-11016.

Hu, W.W., Hu, M., Yuan, B., Jimenez, J.L., Tang, Q., Peng, J.F., Hu, W., Shao, M., Wang, M., Zeng, L.M., Wu, Y.S., Gong, Z.H., Huang, X.F. and He, L.Y. (2013) Insights on organic aerosol aging and the influence of coal combustion at a regional receptor site of central eastern China. Atmos. Chem. Phys. 13, 10095-10112.

IPCC (2013) *Climate Change 2013: The Physical Scientific Basis*. Intergovernmental Panel on Climate Change: Working Group I, Geneva Switzerland

Jaoui, M., Kleindienst, T.E., Lewandowski, M., Offenberg, J.H. and Edney, E.O. (2005) Identification and Quantification of Aerosol Polar Oxygenated Compounds Bearing Carboxylic or Hydroxyl Groups. 2. Organic Tracer Compounds from Monoterpenes. Environ. Sci. Technol. 39, 5661-5673.

Jimenez, J.L., Canagaratna, M.R., Donahue, N.M., Prevot, A.S.H., Zhang, Q., Kroll, J.H., DeCarlo, P.F., Allan, J.D., Coe, H., Ng, N.L., Aiken, A.C., Docherty, K.S., Ulbrich, I.M., Grieshop, A.P., Robinson, A.L., Duplissy, J., Smith, J.D., Wilson, K.R., Lanz, V.A., Hueglin, C., Sun, Y.L., Tian, J., Laaksonen, A., Raatikainen, T., Rautiainen, J., Vaattovaara, P., Ehn, M., Kulmala, M., Tomlinson, J.M., Collins, D.R., Cubison, M.J., Dunlea, E.J., Huffman, J.A., Onasch, T.B., Alfarra, M.R., Williams, P.I., Bower, K., Kondo, Y., Schneider, J., Drewnick, F., Borrmann, S., Weimer, S., Demerjian, K., Salcedo, D., Cottrell, L., Griffin, R., Takami, A., Miyoshi, T., Hatakeyama, S., Shimono, A., Sun, J.Y., Zhang, Y.M., Dzepina, K., Kimmel, J.R., Sueper, D., Jayne, J.T., Herndon, S.C., Trimborn, A.M., Williams, L.R., Wood, E.C., Middlebrook, A.M., Kolb, C.E., Baltensperger, U. and Worsnop, D.R. (2009) Evolution of Organic Aerosols in the Atmosphere. Science 326, 1525-1529.

JRC (2011) *Emission Database for Global Atmospheric Research*. European Commission's Joint Research Centre http://edgar.jrc.ec.europa.eu/overview.php?v=42

Kelly, J.T., Baker, K.R., Nowak, J.B., Murphy, J.G., Markovic, M.Z., VandenBoer, T.C., Ellis, R.A., Neuman, J.A., Weber, R.J. and Roberts, J.M. (2014) Fine-scale simulation of ammonium and nitrate over the South Coast Air Basin and San Joaquin Valley of California during CalNex-2010. Journal of Geophysical Research: Atmospheres 119, 3600-3614.

Kleindienst, T.E., Jaoui, M., Lewandowski, M., Offenberg, J.H. and Docherty, K.S. (2012) The formation of SOA and chemical tracer compounds from the photooxidation of naphthalene and its methyl analogs in the presence and absence of nitrogen oxides. Atmos. Chem. Phys. 12, 8711-8726.

Kleinman, L.I., Daum, P.H., Lee, Y.N., Senum, G.I., Springston, S.R., Wang, J., Berkowitz, C., Hubbe, J., Zaveri, R.A., Brechtel, F.J., Jayne, J., Onasch, T.B. and Worsnop, D. (2007) Aircraft observations of aerosol composition and ageing in New England and Mid-Atlantic States during the summer 2002 New England Air Quality Study field campaign. J. Geophys. Res.-Atmos. 112, D09310.

Knote, C., Hodzic, A., Jimenez, J.L., Volkamer, R., Orlando, J.J., Baidar, S., Brioude, J., Fast, J., Gentner, D.R., Goldstein, A.H., Hayes, P.L., Knighton, W.B., Oetjen, H., Setyan, A., Stark, H., Thalman, R., Tyndall, G., Washenfelder, R., Waxman, E. and Zhang, Q. (2014)

Simulation of semi-explicit mechanisms of SOA formation from glyoxal in aerosol in a 3-D model. Atmos. Chem. Phys. 14, 6213-6239.

Koo, B.Y., Ansari, A.S. and Pandis, S.N. (2003) Integrated approaches to modeling the organic and inorganic atmospheric aerosol components. Atmos. Environ. 37, 4757-4768.

Kroll, J.H., Ng, N.L., Murphy, S.M., Flagan, R.C. and Seinfeld, J.H. (2006) Secondary organic aerosol formation from isoprene photooxidation. Environ. Sci. Technol. 40, 1869-1877.

Lambe, A.T., Onasch, T.B., Croasdale, D.R., Wright, J.P., Martin, A.T., Franklin, J.P., Massoli, P., Kroll, J.H., Canagaratna, M.R., Brune, W.H., Worsnop, D.R. and Davidovits, P. (2012) Transitions from Functionalization to Fragmentation Reactions of Laboratory Secondary Organic Aerosol (SOA) Generated from the OH Oxidation of Alkane Precursors. Environ. Sci. Technol. 46, 5430-5437.

Lewis, C.W., Volckens, J., Braddock, J.N., Crews, W.S., Lonneman, W.A. and McNichol, A.P. (2006) Absence of 14C in PM2.5 Emissions from Gasohol Combustion in Small Engines. Aerosol Sci. Technol. 40, 657-663.

Lim, H.J., Carlton, A.G. and Turpin, B.J. (2005) Isoprene forms secondary organic aerosol through cloud processing: Model simulations. Environ. Sci. Technol. 39, 4441-4446.

Martin-Reviejo, M. and Wirtz, K. (2005) Is benzene a precursor for secondary organic aerosol? Environ. Sci. Technol. 39, 1045-1054.

Matsunaga, A. and Ziemann, P.J. (2010) Gas-Wall Partitioning of Organic Compounds in a Teflon Film Chamber and Potential Effects on Reaction Product and Aerosol Yield Measurements. Aerosol Sci. Technol. 44, 881-892.

McKeen, S., Chung, S.H., Wilczak, J., Grell, G., Djalalova, I., Peckham, S., Gong, W., Bouchet, V., Moffet, R., Tang, Y., Carmichael, G.R., Mathur, R. and Yu, S. (2007) Evaluation of several PM(2.5) forecast models using data collected during the ICARTT/NEAQS 2004 field study. J. Geophys. Res.-Atmos. 112.

Middlebrook, A.M., Bahreini, R., Jimenez, J.L. and Canagaratna, M.R. (2012) Evaluation of Composition-Dependent Collection Efficiencies for the Aerodyne Aerosol Mass Spectrometer using Field Data. Aerosol Sci. Technol. 46, 258-271.

Mohr, C., DeCarlo, P.F., Heringa, M.F., Chirico, R., Slowik, J.G., Richter, R., Reche, C., Alastuey, A., Querol, X., Seco, R., Peñuelas, J., Jiménez, J.L., Crippa, M., Zimmermann, R., Baltensperger, U. and Prévôt, A.S.H. (2011) Identification and quantification of organic aerosol from cooking and other sources in Barcelona using aerosol mass spectrometer data. Atmos. Chem. Phys. 11, 1649-1665.

Murphy, B.N., Donahue, N.M., Fountoukis, C. and Pandis, S.N. (2011) Simulating the oxygen content of ambient organic aerosol with the 2D volatility basis set. Atmos. Chem. Phys. 11, 7859-7873.

Murphy, D.M., Cziczo, D.J., Froyd, K.D., Hudson, P.K., Matthew, B.M., Middlebrook, A.M., Peltier, R.E., Sullivan, A., Thomson, D.S. and Weber, R.J. (2006) Single-particle mass spectrometry of tropospheric aerosol particles. Journal of Geophysical Research: Atmospheres 111, D23S32.

Ortega, A.M., Day, D.A., Cubison, M.J., Brune, W.H., Bon, D., de Gouw, J.A. and Jimenez, J.L. (2013) Secondary organic aerosol formation and primary organic aerosol oxidation from biomass-burning smoke in a flow reactor during FLAME-3. Atmos. Chem. Phys. 13, 11551-11571.

Parrish, D.D., Stohl, A., Forster, C., Atlas, E.L., Blake, D.R., Goldan, P.D., Kuster, W.C. and de Gouw, J.A. (2007) Effects of mixing on evolution of hydrocarbon ratios in the troposphere. J. Geophys. Res.-Atmos. 112, D10S34.

Perraud, V., Bruns, E.A., Ezell, M.J., Johnson, S.N., Yu, Y., Alexander, M.L., Zelenyuk, A., Imre, D., Chang, W.L., Dabdub, D., Pankow, J.F. and Finlayson-Pitts, B.J. (2012) Nonequilibrium atmospheric secondary organic aerosol formation and growth. Proc. Natl. Acad. Sci. U. S. A. 109, 2836-2841.

Pye, H.O.T. and Seinfeld, J.H. (2010) A global perspective on aerosol from low-volatility organic compounds. Atmos. Chem. Phys. 10, 4377-4401.

Robinson, A.L., Donahue, N.M., Shrivastava, M.K., Weitkamp, E.A., Sage, A.M., Grieshop, A.P., Lane, T.E., Pierce, J.R. and Pandis, S.N. (2007) Rethinking organic aerosols: Semivolatile emissions and photochemical aging. Science 315, 1259-1262.

Ryerson, T.B., Andrews, A.E., Angevine, W.M., Bates, T.S., Brock, C.A., Cairns, B., Cohen, R.C., Cooper, O.R., de Gouw, J.A., Fehsenfeld, F.C., Ferrare, R.A., Fischer, M.L., Flagan, R.C., Goldstein, A.H., Hair, J.W., Hardesty, R.M., Hostetler, C.A., Jimenez, J.L., Langford, A.O., McCauley, E., McKeen, S.A., Molina, L.T., Nenes, A., Oltmans, S.J., Parrish, D.D., Pederson, J.R., Pierce, R.B., Prather, K., Quinn, P.K., Seinfeld, J.H., Senff, C.J., Sorooshian, A., Stutz, J., Surratt, J.D., Trainer, M., Volkamer, R., Williams, E.J. and Wofsy, S.C. (2013) The 2010 California Research at the Nexus of Air Quality and Climate Change (CalNex) field study. J. Geophys. Res.-Atmos. 118, 5830-5866.

Sarwar, G., Fahey, K., Kwok, R., Gilliam, R.C., Roselle, S.J., Mathur, R., Xue, J., Yu, J. and Carter, W.P.L. (2013) Potential impacts of two SO2 oxidation pathways on regional sulfate concentrations: Aqueous-phase oxidation by NO2 and gas-phase oxidation by Stabilized Criegee Intermediates. Atmos. Environ. 68, 186-197.

Saukko, E., Lambe, A.T., Massoli, P., Koop, T., Wright, J.P., Croasdale, D.R., Pedernera, D.A., Onasch, T.B., Laaksonen, A., Davidovits, P., Worsnop, D.R. and Virtanen, A. (2012) Humidity-dependent phase state of SOA particles from biogenic and anthropogenic precursors. Atmos. Chem. Phys. 12, 7517-7529.

Schauer, J.J., Kleeman, M.J., Cass, G.R. and Simoneit, B.R.T. (1999) Measurement of emissions from air pollution sources. 1. C-1 through C-29 organic compounds from meat charbroiling. Environ. Sci. Technol. 33, 1566-1577.

Skamarock, W.C., Klemp, J.B., Dudhia, J., Gill, D.O., Barker, D.M., Duda, M.G., Huang, X., Wang, W. and Powers, J.G. (2008) A description of the Advanced Reserch WRF version 3. NCAR Technical Note NCAR/TN-475+STR.

Slowik, J.G., Stroud, C., Bottenheim, J.W., Brickell, P.C., Chang, R.Y.W., Liggio, J., Makar, P.A., Martin, R.V., Moran, M.D., Shantz, N.C., Sjostedt, S.J., van Donkelaar, A., Vlasenko, A., Wiebe, H.A., Xia, A.G., Zhang, J., Leaitch, W.R. and Abbatt, J.P.D. (2010) Characterization of a large biogenic secondary organic aerosol event from eastern Canadian forests. Atmos. Chem. Phys. 10, 2825-2845.

Spracklen, D.V., Jimenez, J.L., Carslaw, K.S., Worsnop, D.R., Evans, M.J., Mann, G.W., Zhang, Q., Canagaratna, M.R., Allan, J., Coe, H., McFiggans, G., Rap, A. and Forster, P. (2011) Aerosol mass spectrometer constraint on the global secondary organic aerosol budget. Atmos. Chem. Phys. 11, 12109-12136.

Sun, Y.L., Zhang, Q., Schwab, J.J., Demerjian, K.L., Chen, W.N., Bae, M.S., Hung, H.M., Hogrefe, O., Frank, B., Rattigan, O.V. and Lin, Y.C. (2011) Characterization of the

sources and processes of organic and inorganic aerosols in New York city with a high-resolution time-of-flight aerosol mass apectrometer. Atmos. Chem. Phys. 11, 1581-1602.

Szmigielski, R., Surratt, J.D., Gómez-González, Y., Van der Veken, P., Kourtchev, I., Vermeylen, R., Blockhuys, F., Jaoui, M., Kleindienst, T.E., Lewandowski, M., Offenberg, J.H., Edney, E.O., Seinfeld, J.H., Maenhaut, W. and Claeys, M. (2007) 3-methyl-1,2,3-butanetricarboxylic acid: An atmospheric tracer for terpene secondary organic aerosol. Geophys. Res. Lett. 34, L24811.

Tsimpidi, A.P., Karydis, V.A., Zavala, M., Lei, W., Molina, L., Ulbrich, I.M., Jimenez, J.L. and Pandis, S.N. (2010) Evaluation of the volatility basis-set approach for the simulation of organic aerosol formation in the Mexico City metropolitan area. Atmos. Chem. Phys. 10, 525-546.

Tunved, P., Hansson, H.C., Kerminen, V.M., Strom, J., Dal Maso, M., Lihavainen, H., Viisanen, Y., Aalto, P.P., Komppula, M. and Kulmala, M. (2006) High natural aerosol loading over boreal forests. Science 312, 261-263.

Volkamer, R., Jimenez, J.L., Martini, F.S., Dzepina, K., Zhang, Q., Salcedo, D., Molina, L.T., Worsnop, D.R. and Molina., M.J. (2006) Secondary Organic Aerosol Formation from Anthropogenic Air Pollution: Rapid and Higher than Expected. Geophys. Res. Lett. 33, L17811.

Volkamer, R., San Martini, F., Molina, L.T., Salcedo, D., Jimenez, J.L. and Molina, M.J. (2007) A missing sink for gas-phase glyoxal in Mexico City: Formation of secondary organic aerosol. Geophys. Res. Lett. 34, L19807.

Volkamer, R., Ziemann, P.J. and Molina, M.J. (2009) Secondary Organic Aerosol Formation from Acetylene (C(2)H(2)): seed effect on SOA yields due to organic photochemistry in the aerosol aqueous phase. Atmos. Chem. Phys. 9, 1907-1928.

Wang, Q., Shao, M., Zhang, Y., Wei, Y., Hu, M. and Guo, S. (2009) Source apportionment of fine organic aerosols in Beijing. Atmos. Chem. Phys. 9, 8573-8585.

Warneke, C., de Gouw, J.A., Holloway, J.S., Peischl, J., Ryerson, T.B., Atlas, E., Blake, D., Trainer, M. and Parrish, D.D. (2012) Multiyear trends in volatile organic compounds in Los Angeles, California: Five decades of decreasing emissions. J. Geophys. Res.-Atmos. 117, D00V17.

Warneke, C., McKeen, S.A., de Gouw, J.A., Goldan, P.D., Kuster, W.C., Holloway, J.S., Williams, E.J., Lerner, B.M., Parrish, D.D., Trainer, M., Fehsenfeld, F.C., Kato, S., Atlas, E.L., Baker, A. and Blake, D.R. (2007) Determination of urban volatile organic compound emission ratios and comparison with an emissions database. J. Geophys. Res.-Atmos. 112, D10S47.

Washenfelder, R.A., Young, C.J., Brown, S.S., Angevine, W.M., Atlas, E.L., Blake, D.R., Bon, D.M., Cubison, M.J., de Gouw, J.A., Dusanter, S., Flynn, J., Gilman, J.B., Graus, M., Griffith, S., Grossberg, N., Hayes, P.L., Jimenez, J.L., Kuster, W.C., Lefer, B.L., Pollack, I.B., Ryerson, T.B., Stark, H., Stevens, P.S. and Trainer, M.K. (2011) The glyoxal budget and its contribution to organic aerosol for Los Angeles, California, during CalNex 2010. J. Geophys. Res.-Atmos. 116, D00V02.

Watson, J.G. (2002) Visibility: Science and regulation. J. Air Waste Manage. Assoc. 52, 628-713.

Yarwood, G., Jung, J., Whitten, G.Z., Heo, G., Mellberg, J., Estes, E. (2010) *Updates to the Carbon Bond Mechanism for Version 6 (CB6). Presented at the 9th Annual CMAS*

Conference, Chapel, Hill, NC. ENVIRON International Corporation, Novato http://www.camx.com/publ/pdfs/CB05_Final_Report_120805.pdf

Yatavelli, R.L.N., Stark, H., Thompson, S.L., Kimmel, J.R., Cubison, M.J., Day, D.A., Campuzano-Jost, P., Palm, B.B., Hodzic, A., Thornton, J.A., Jayne, J.T., Worsnop, D.R. and Jimenez, J.L. (2014) Semicontinuous measurements of gas–particle partitioning of organic acids in a ponderosa pine forest using a MOVI-HRToF-CIMS. Atmos. Chem. Phys. 14, 1527-1546.

Zhang, Q., Jimenez, J.L., Canagaratna, M.R., Allan, J.D., Coe, H., Ulbrich, I., Alfarra, M.R., Takami, A., Middlebrook, A.M., Sun, Y.L., Dzepina, K., Dunlea, E., Docherty, K., DeCarlo, P.F., Salcedo, D., Onasch, T., Jayne, J.T., Miyoshi, T., Shimono, A., Hatakeyama, S., Takegawa, N., Kondo, Y., Schneider, J., Drewnick, F., Borrmann, S., Weimer, S., Demerjian, K., Williams, P., Bower, K., Bahreini, R., Cottrell, L., Griffin, R.J., Rautiainen, J., Sun, J.Y., Zhang, Y.M. and Worsnop, D.R. (2007) Ubiquity and dominance of oxygenated species in organic aerosols in anthropogenically-influenced Northern Hemisphere midlatitudes. Geophys. Res. Lett. 34, L13801.

Zhang, X., Cappa, C.D., Jathar, S.H., McVay, R.C., Ensberg, J.J., Kleeman, M.J. and Seinfeld, J.H. (2014) Influence of vapor wall loss in laboratory chambers on yields of secondary organic aerosol. Proc. Natl. Acad. Sci. U. S. A.

Zhang, X., Liu, J., Parker, E.T., Hayes, P.L., Jimenez, J.L., de Gouw, J.A., Flynn, J.H., Grossberg, N., Lefer, B.L. and Weber, R.J. (2012) On the gas-particle partitioning of soluble organic aerosol in two urban atmospheres with contrasting emissions: 1. Bulk water-soluble organic carbon. J. Geophys. Res.-Atmos. 117, D00V16.

Zotter, P., El-Haddad, I., Zhang, Y., Hayes, P.L., Zhang, X., Lin, Y.-H., Wacker, L., Schnelle-Kreis, J., Abbaszade, G., Zimmermann, R., Surratt, J.D., Weber, R., Jimenez, J.L., Szidat, S., Baltensperger, U. and Prévôt, A.S.H. (2014) Diurnal cycle of fossil and nonfossil carbon using radiocarbon analyses during CalNex. Journal of Geophysical Research: Atmospheres, 2013JD021114.

Supplemental Information for:

Modeling the formation and aging of secondary organic aerosols in Los Angeles during CalNex 2010

Patrick L. Hayes[1,2,*], Annmarie G. Carlton[3], Kirk R. Baker[4], Ravan Ahmadov[1,5], Rebecca A. Washenfelder[1,5], Sergio Alvarez[6], Bernhard Rappenglück[6], Jessica B. Gilman[1,5], William C. Kuster[5], Joost A. de Gouw[1,5], Peter Zotter[7], Andre S. H. Prévôt[7], Sönke Szidat[8], Tadeusz E. Kleindienst[4], John H. Offenberg[4], Jose L. Jimenez[1,2]

(1) Cooperative Institute for Research in Environmental Sciences (CIRES), University of Colorado, Boulder, CO, USA.
(2) Department of Chemistry and Biochemistry, University of Colorado, Boulder, CO, USA.
(3) Department of Environmental Sciences, Rutgers University, New Brunswick, NJ, USA.
(4) US Environmental Protection Agency, Research Triangle Park, NC, USA.
(5) Earth System Research Laboratory, National Oceanic and Atmospheric Administration (NOAA), Boulder, CO, USA.
(6) Department of Earth and Atmospheric Sciences, University of Houston, TX, USA.
(7) Laboratory of Atmospheric Chemistry, Paul Scherrer Institute, Villigen, Switzerland.
(8) Department of Chemistry and Biochemistry & Oeschger Centre for Climate Change Research, University of Bern, Switzerland.
*: Now at Université de Montréal, Department of Chemistry, Montreal, QC, CANADA
Correspondence to: J. L. Jimenez (jose.jimenez@colorado.edu)

Figure Captions

Table SI-1. Summary of the VOCs and parameters used to model the formation of SOA (Atkinson and Arey, 2003; Carter, 2010; Tsimpidi et al., 2010). All aging of VOCs after the initial oxidation reaction occurs with a gas-phase rate constant of $k_{OH} = 1 \times 10^{-11}$ cm^3 $molec^{-1}$ s^{-1}. Note that the aging rate constant was erroneously reported as 4×10^{-11} cm^3 $molec^{-1}$ s^{-1} in Tsimpidi et al. All SOA from VOCs has a ΔH_{vap} of 36 kJ mol^{-1} (Volkamer et al., 2006).

Table SI-2. Summary of the Robinson et al. (2007) and the Grieshop et al. (2009) parameterizations for P-S/IVOCs.

Figure SI-1. The evolution of OA/ΔCO versus photochemical age for CalNex separated by cloudy days and mostly clear days. The enhanced CO (ΔCO) is calculated as the difference of the ambient CO and the background CO (105 ppb) (Hayes et al., 2013). The cloudy days are 17 and 27 May 2010, as well as 11 June 2010.

Figure SI-2. Model/measurement comparisons of the diurnal cycles for selected VOC mixing ratios as well as for POA mass concentrations. Note that for the VOCs the GRI, ROB, PYE, ROB + 4xV parameterizations give the same results.

Figure SI-3. (Top) Scatter plots for naphthalene, 1-methylnaphthalene, and 2-methylnaphthalene versus CO mixing ratios. Data includes only measurements from 00:00 – 06:00 (local time) to minimize the impact of photochemical oxidation on the PAH concentrations. Also shown in the top panels are the ODR linear regression analyses of the data with the y-intercept fixed at 105 ppb CO, which is the background CO concentration (Hayes et al., 2013). For more information on the methodology used to measure naphthalene and the methylnaphthalenes see Presto et al. (2012; 2011). **(Bottom)** Model and measurement diurnal cycles for naphthalene, 1-methylnaphthalene, and 2-methylnaphthalene.

Figure SI-4. Anthropogenic CO fluxes on a 12 km grid in Southern California that are used in the WRF-Chem simulation. The box indicates the region around LA where the emissions of atmospheric species are set to zero in order to determine the concentration of background SOA.

Figure SI-5. Model/measurement comparison of SOA mass concentrations after excluding from the model P-S/IVOC, or, in the case of the PYE variation, SVOC emissions from cooking-related activities. Otherwise the figure is identical to Figure 3 in the main text.

Figure SI-6: (A) The estimated mass concentration of SOA from gasoline vehicles, diesel vehicles, cooking emissions, in-basin biogenic emissions, and the regional background (brown)

plotted by time-of-day. **(B)** The fractional contribution of each source plotted by time of day. **(C)** Average fractional contribution from each source.

Figure SI-7: Scatter plots of **(A)** benzene, **(B)** low-yield aromatic VOCs, and **(C)** high-yield aromatic VOCs measured by GC-MS against the concentration predicted by WRF-CMAQ. The low-yield aromatics correspond to the family ARO1 and the high-yield aromatics to the family ARO2 in Table SI-1. Also shown for reference are the 5:1, 1:1, and 1:5 lines. **(D)** SOA/ΔCO as a function of photochemical age as determined by measurements (black circles) and predicted by WRF-CMAQ (red squares). The left and right axes are plotted on different scales for clarity. Photochemical age is determined from the ratio of NO_Y to NO_X (Hayes et al., 2013).

Figure SI-8: Time series of inorganic and organic aerosols at the Pasadena ground site during CalNex measured by an AMS or modeled by WRF-CMAQ. For SOA the concentration was determined using positive matrix factorization analysis of the AMS measurements. The AMS measurements have a PM_1 size cut, and the WRF-CMAQ model results are the sum of the Aiken and accumulation modes, which corresponds to $PM_{2.5}$. (Note: In WRF-CMAQ all SOA species are assigned to the accumulation mode.)

Figure SI-9: Scatter plots of the inorganic aerosol measurements from an AMS against the modeled concentrations from WRF-CMAQ. The data shown are the same as in Figure SI-7. Also shown are the corresponding ODR linear regression analyses and corresponding fit parameters.

References

Atkinson, R. and Arey, J. (2003) Atmospheric degradation of volatile organic compounds. Chem. Rev. 103, 4605-4638.

Carter, W.P.L. (2010) Development of the SAPRC-07 chemical mechanism. Atmos. Environ. 44, 5324-5335.

Grieshop, A.P., Logue, J.M., Donahue, N.M. and Robinson, A.L. (2009) Laboratory investigation of photochemical oxidation of organic aerosol from wood fires 1: measurement and simulation of organic aerosol evolution. Atmos. Chem. Phys. 9, 1263-1277.

Hayes, P.L., Ortega, A.M., Cubison, M.J., Froyd, K.D., Zhao, Y., Cliff, S.S., Hu, W.W., Toohey, D.W., Flynn, J.H., Lefer, B.L., Grossberg, N., Alvarez, S., Rappenglück, B., Taylor, J.W., Allan, J.D., Holloway, J.S., Gilman, J.B., Kuster, W.C., de Gouw, J.A., Massoli, P., Zhang, X., Liu, J., Weber, R.J., Corrigan, A.L., Russell, L.M., Isaacman, G., Worton, D.R., Kreisberg, N.M., Goldstein, A.H., Thalman, R., Waxman, E.M., Volkamer, R., Lin, Y.H., Surratt, J.D., Kleindienst, T.E., Offenberg, J.H., Dusanter, S., Griffith, S., Stevens, P.S., Brioude, J., Angevine, W.M. and Jimenez, J.L. (2013) Organic aerosol composition and sources in Pasadena, California during the 2010 CalNex campaign. J. Geophys. Res.-Atmos., 9233-9257.

Presto, A.A., Hennigan, C.J., Nguyen, N.T. and Robinson, A.L. (2012) Determination of Volatility Distributions of Primary Organic Aerosol Emissions from Internal Combustion Engines Using Thermal Desorption Gas Chromatography Mass Spectrometry. Aerosol Sci. Technol. 46, 1129-1139.

Presto, A.A., Nguyen, N.T., Ranjan, M., Reeder, A.J., Lipsky, E.M., Hennigan, C.J., Miracolo, M.A., Riemer, D.D. and Robinson, A.L. (2011) Fine particle and organic vapor emissions from staged tests of an in-use aircraft engine. Atmos. Environ. 45, 3603-3612.

Robinson, A.L., Donahue, N.M., Shrivastava, M.K., Weitkamp, E.A., Sage, A.M., Grieshop, A.P., Lane, T.E., Pierce, J.R. and Pandis, S.N. (2007) Rethinking organic aerosols: Semivolatile emissions and photochemical aging. Science 315, 1259-1262.

Tsimpidi, A.P., Karydis, V.A., Zavala, M., Lei, W., Molina, L., Ulbrich, I.M., Jimenez, J.L. and Pandis, S.N. (2010) Evaluation of the volatility basis-set approach for the simulation of organic aerosol formation in the Mexico City metropolitan area. Atmos. Chem. Phys. 10, 525-546.

Volkamer, R., Jimenez, J.L., San Martini, F., Dzepina, K., Zhang, Q., Salcedo, D., Molina, L.T., Worsnop, D.R. and Molina, M.J. (2006) Secondary organic aerosol formation from anthropogenic air pollution: Rapid and higher than expected. Geophys. Res. Lett. 33, L17811.

Table 1

AMS	Aerosol Mass Spectrometer
BG-SOA	Background secondary organic aerosols
CalNex	California research at the nexus of air quality and climate change field campaign
WRF-CMAQ	Weather Research Forecasting – Community multiscale air quality model
GRI	Grieshop et al. (2009) parameterization for secondary organic aerosol formation from P-S/IVOCs
IVOCs	Intermediate volatility organic compounds
OA	Organic aerosol
ODR	Orthogonal distance regression
PAH	Polycyclic aromatic hydrocarbon
PBL	Planetary Boundary Layer
P-S/IVOCs	Primary semi-volatile and intermediate volatility organic compounds
PYE	Pye and Seinfeld (2010) parameterization for secondary organic aerosols formation from P-S/IVOCs
ROB	Robinson et al. (2007) parameterization for secondary organic aerosol formation from P-S/IVOCs
SI-SOA	Secondary organic aerosol from primary semi-volatile and intermediate volatility organic compounds
SOA	Secondary organic aerosol
SVOCs	Semi-volatile organic compounds
V-SOA	Secondary organic aerosol formed from the oxidation of volatile organic compounds
VBS	Volatility basis set
VOCs	Volatile organic compounds
ΔCO	Enhanced carbon monoxide concentration over the background concentration (105 ppb).

Table 2

Model Name	Variation	Notes	References	Figures showing data specific to model
Box Model	1 (ROB)	VOCs: Tsimpidi et al. parameterization with aging, P-S/IVOCs: Robinson et al. parameterization, and all SOA treated within VBS framework.	Tsimpidi et al. *Atmos. Chem. Phys.* **2010,** 525-546. Robinson et al. *Science* **2007,** 1259-1262.	3, 6, 8, SI-1, SI-4
	2 (GRI)	VOCs: Tsimpidi et al. parameterization with aging, P-S/IVOCs: Grieshop et al. parameterization, and all SOA treated within VBS framework.	Tsimpidi et al. *Atmos. Chem. Phys.* **2010,** 525-546. Grieshop et al. *Science* **2009,** 1263-1277.	3, 4, 5, 6, 8, SI-1, SI-4, SI-5
	3 (PYE)	VOCs: Tsimpidi et al. parameterization with aging, P-S/IVOCs: Pye and Seinfeld parameterization.	Tsimpidi et al. *Atmos. Chem. Phys.* **2010,** 525-546. Pye and Seinfeld *Atmos. Chem. Phys.* **2010,** 4377-4401.	3, 6, SI-1, SI-4
	4 (ROB + 4xV)	VOCs: Tsimpidi et al. parameterization without aging and aromatic yield multiplied by 4, P-S/IVOCs: Robinson et al. parameterization, and all SOA treated within VBS framework.	Tsimpidi et al. *Atmos. Chem. Phys.* **2010,** 525-546. Robinson et al. *Science* **2007,** 1259-1262. Zhang et al. *PNAS* **2014**.	3, 6, SI-4
	5	VOCs: Koo et al. and Ng et al. wherein SOA is treated in a lumped product parameterization.	Koo et al. *Atmos. Environ.* **2003,** 4757-4768. Ng et al. *Atmos. Chem. Phys.* **2007,** 3909-3922.	7

Table 2 (cont.)

Model Name	Variation	Notes	References	Relevant figures showing data specific to model
WRF-CMAQ	v5.0.1	4 anthropogenic VOC and 3 biogenic VOC precursors and GLY/MGLY. 12 semi-volatile partitioning species and 7 non-volatile SOA species	Carlton et al. *Environ. Sci. Technol.* **2010,** 8553-8560.	7, SI-6, SI-7
'Simple' Model	N/A	Single lumped precursor and single lumped, non-volatile SOA product.	Hodzic et al. *Geosci. Model Dev.* **2011,** 901-917.	9, 10
WRF-Chem	N/A	4-bin VBS framework with aging, 7 anthropogenic VOC classes and 4 biogenic VOC classes	Ahmadov et al. *J. Geophys. Res.-Atmos.* **2012,** D06301.	2, SI-3

Table 3

Measurement	Technique	Uncertainty	Reference
Bulk aerosol mass concentrations for organics, nitrate, sulfate, and ammonium as well as the concentrations of organic aerosol components	High-resolution Aerosol Mass Spectrometry (AMS) and Positive Matrix Factorization (PMF) analysis	±30%	Hayes et al. 2013
Oxygen-to-carbon ratio	High-resolution Aerosol Mass Spectrometer (AMS) and Elemental Analysis (EA)	±30%	Hayes et al. 2013
Speciated VOCs	Gas chromatography – mass spectrometry	±5 – 25% (hydrocarbons) ±20 – 35% (oxygenates)	Borbon et al. 2013
CO	VUV Fluorescence	±4%	Hayes et al. 2013
Modern and fossil fraction of organic carbon	^{14}C	See text	Zotter et al. 2014
Concentration of SOA from specific precursor compounds	U.S. E.P.A. tracer method and measurement of oxygenates from filter samples using GC-MS	See text	Kleindienst et al. 2013
Concentration of naphthalene and its derivatives	Thermal desorption gas chromatography mass spectrometry	±30%	Presto et al. 2011 Presto et al. 2012

Table 4

Variation	SOA / ΔCO slope between 0 and 0.25 Days	SOA / ΔCO slope between 0.25 and 0.5 Days
Observed (Hayes et al. 2013)	108 μg m^{-3}	
ROB	69 μg m^{-3} $ppmv^{-1}$	88 μg m^{-3} $ppmv^{-1}$
GRI	110 μg m^{-3} $ppmv^{-1}$	130 μg m^{-3} $ppmv^{-1}$
PYE	168 μg m^{-3} $ppmv^{-1}$	153 μg m^{-3} $ppmv^{-1}$
ROB + 4xV	105 μg m^{-3} $ppmv^{-1}$	123 μg m^{-3} $ppmv^{-1}$

Figure 1

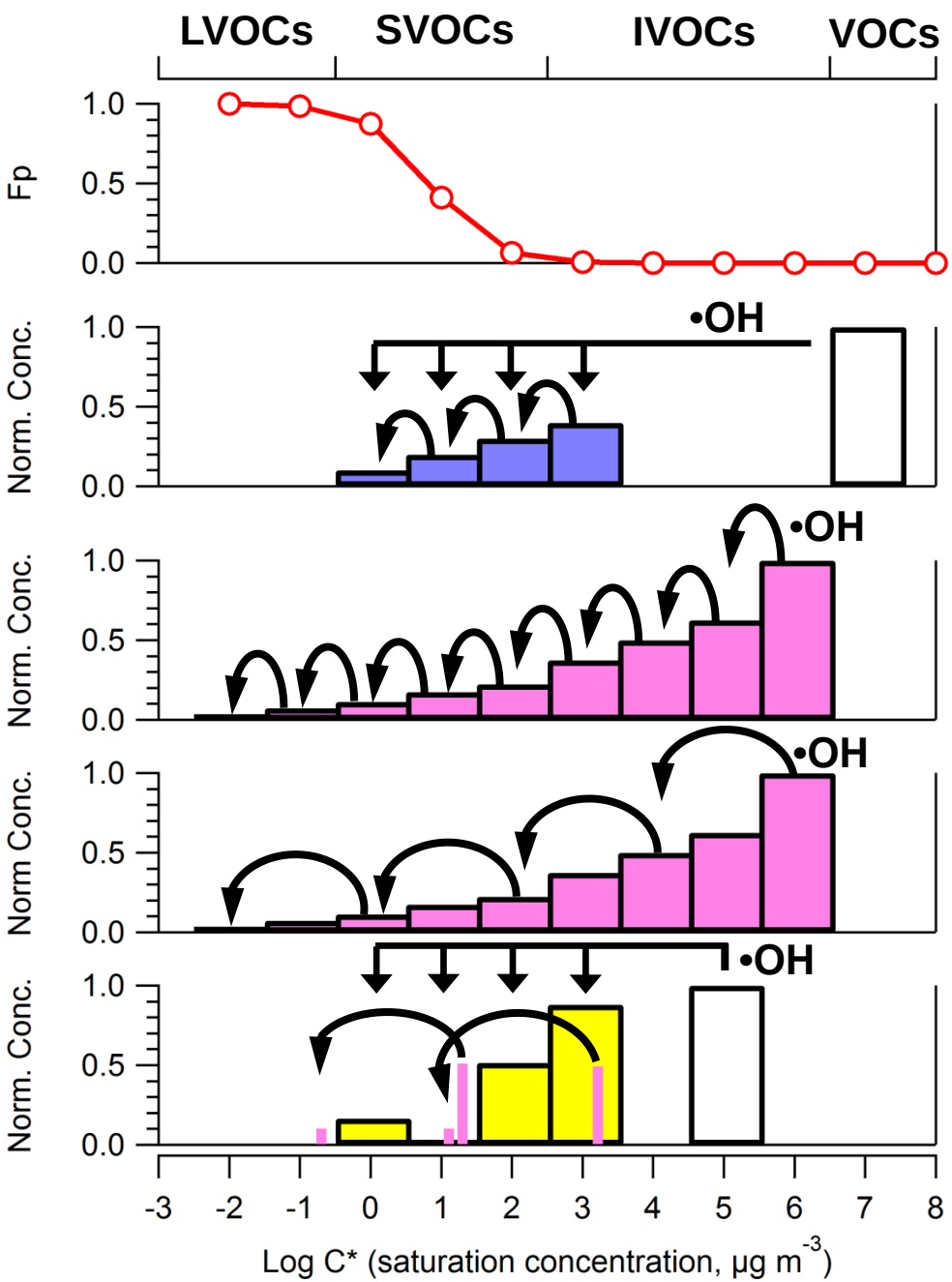

Reference	Precursors
Tsimpidi et al.	46 VOCs
Robinson et al.	Primary S/IVOCs
Grieshop et al.	Primary S/IVOCs
Pye & Seinfeld	Primary S/IVOCs

Figure 2

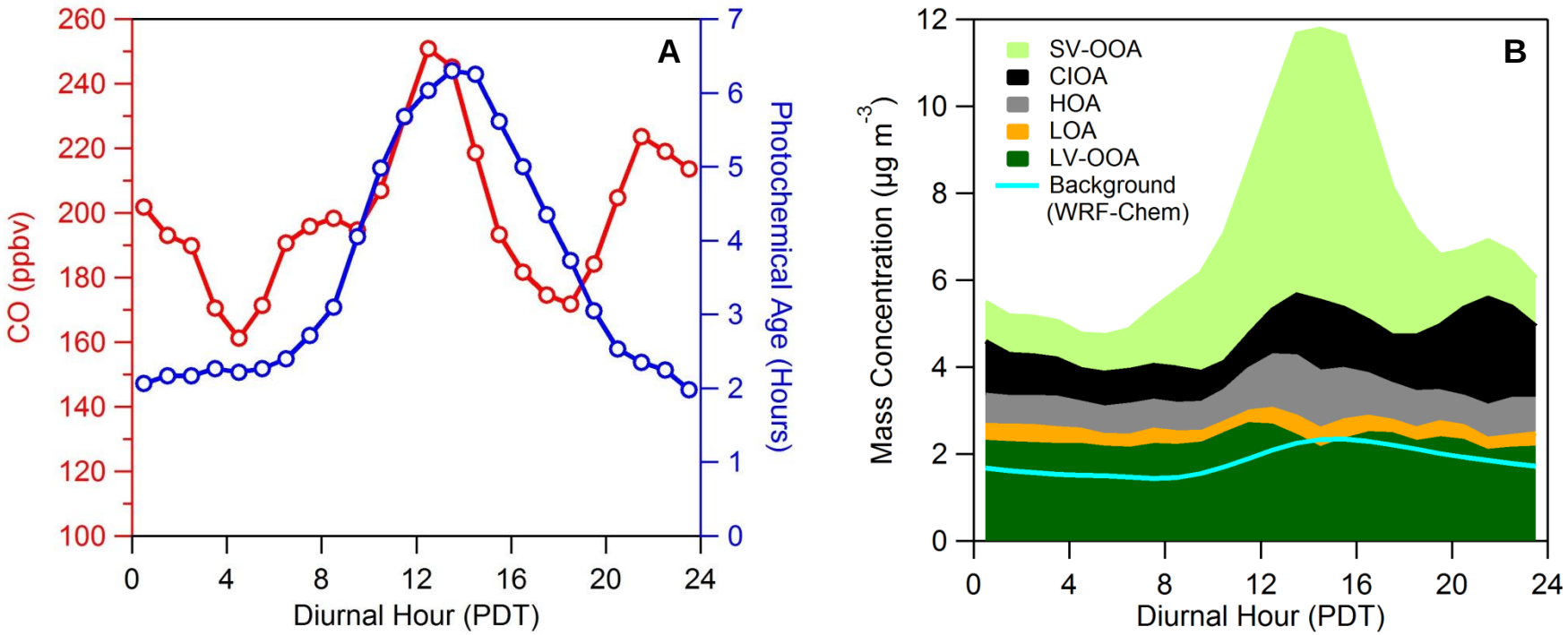
A
CO (ppbv)
Photochemical Age (Hours)
Diurnal Hour (PDT)
B
SV-OOA
CIOA
HOA
LOA
LV-OOA
Background
(WRF-Chem)
Mass Concentration (µg m-3)
Diurnal Hour (PDT)

Figure 3

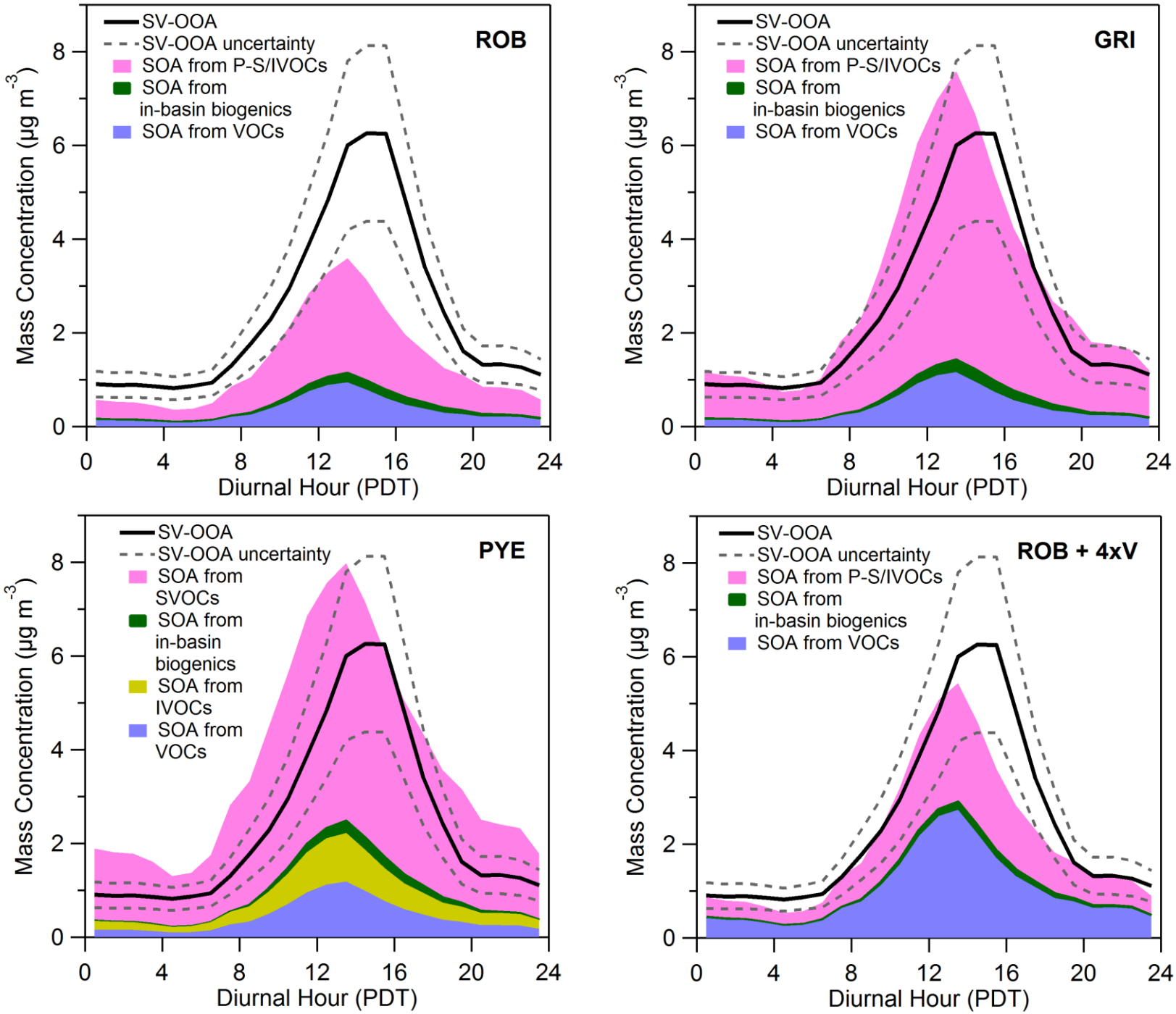
ROB
SV-OOA
SV-OOA uncertainty
SOA from P-S/IVOCs
SOA from in-basin biogenics
SOA from VOCs
GRI
SV-OOA
SV-OOA uncertainty
SOA from P-S/IVOCs
SOA from in-basin biogenics
SOA from VOCs
PYE
SV-OOA
SV-OOA uncertainty
SOA from SVOCs
SOA from in-basin biogenics
SOA from IVOCs
SOA from VOCs
ROB + 4xV
SV-OOA
SV-OOA uncertainty
SOA from P-S/IVOCs
SOA from in-basin biogenics
SOA from VOCs
Mass Concentration (µg m-3)
Diurnal Hour (PDT)
0
2
4
6
8
0
4
8
12
16
20
24

Figure 4

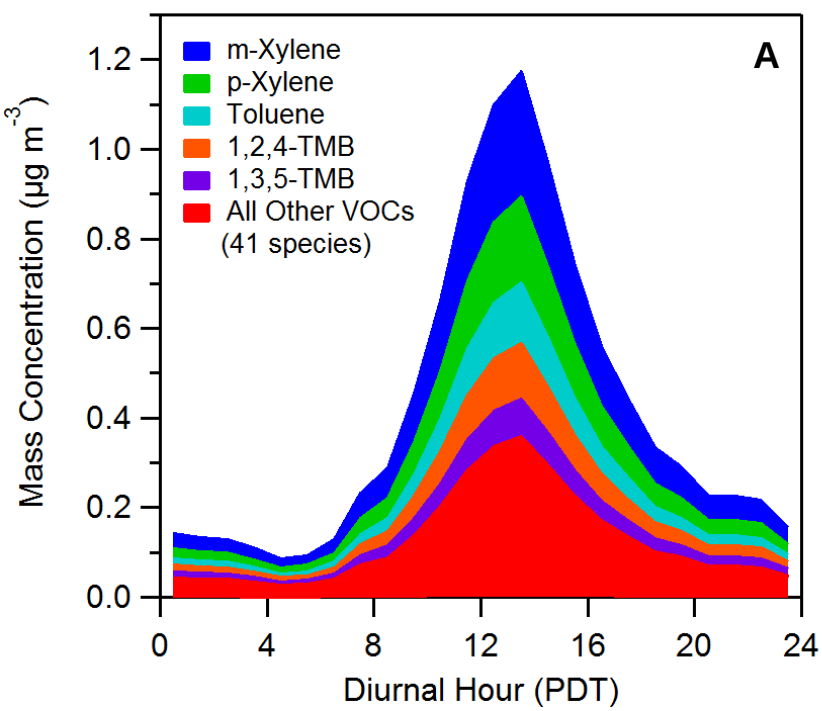
A
m-Xylene
p-Xylene
Toluene
1,2,4-TMB
1,3,5-TMB
All Other VOCs
(41 species)
Mass Concentration (µg m-3)
1.2
1.0
0.8
0.6
0.4
0.2
0.0
0
4
8
12
16
20
24
Diurnal Hour (PDT)

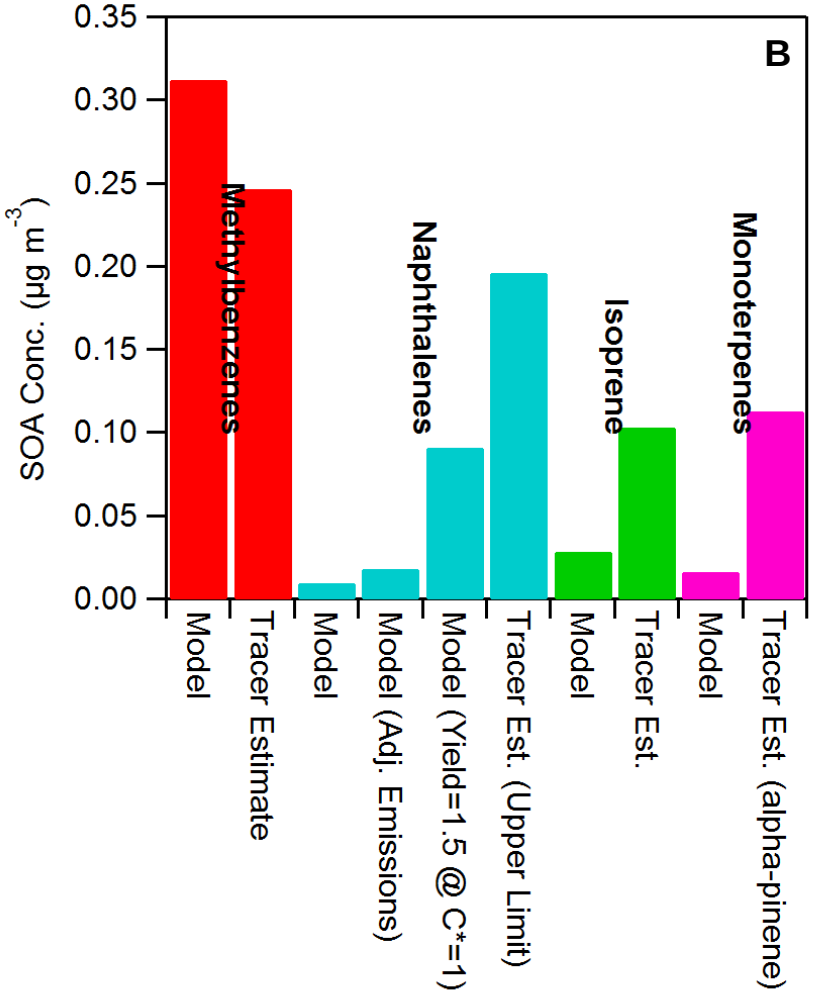
B
SOA Conc. (µg m-3)
0.35
0.30
0.25
0.20
0.15
0.10
0.05
0.00
Methylbenzenes
Naphthalenes
Isoprene
Monoterpenes
Model
Tracer Estimate
Model
Model (Adj. Emissions)
Model (Yield=1.5 @ C*=1)
Tracer Est. (Upper Limit)
Model
Tracer Est.
Model
Tracer Est. (alpha-pinene)

Figure 5

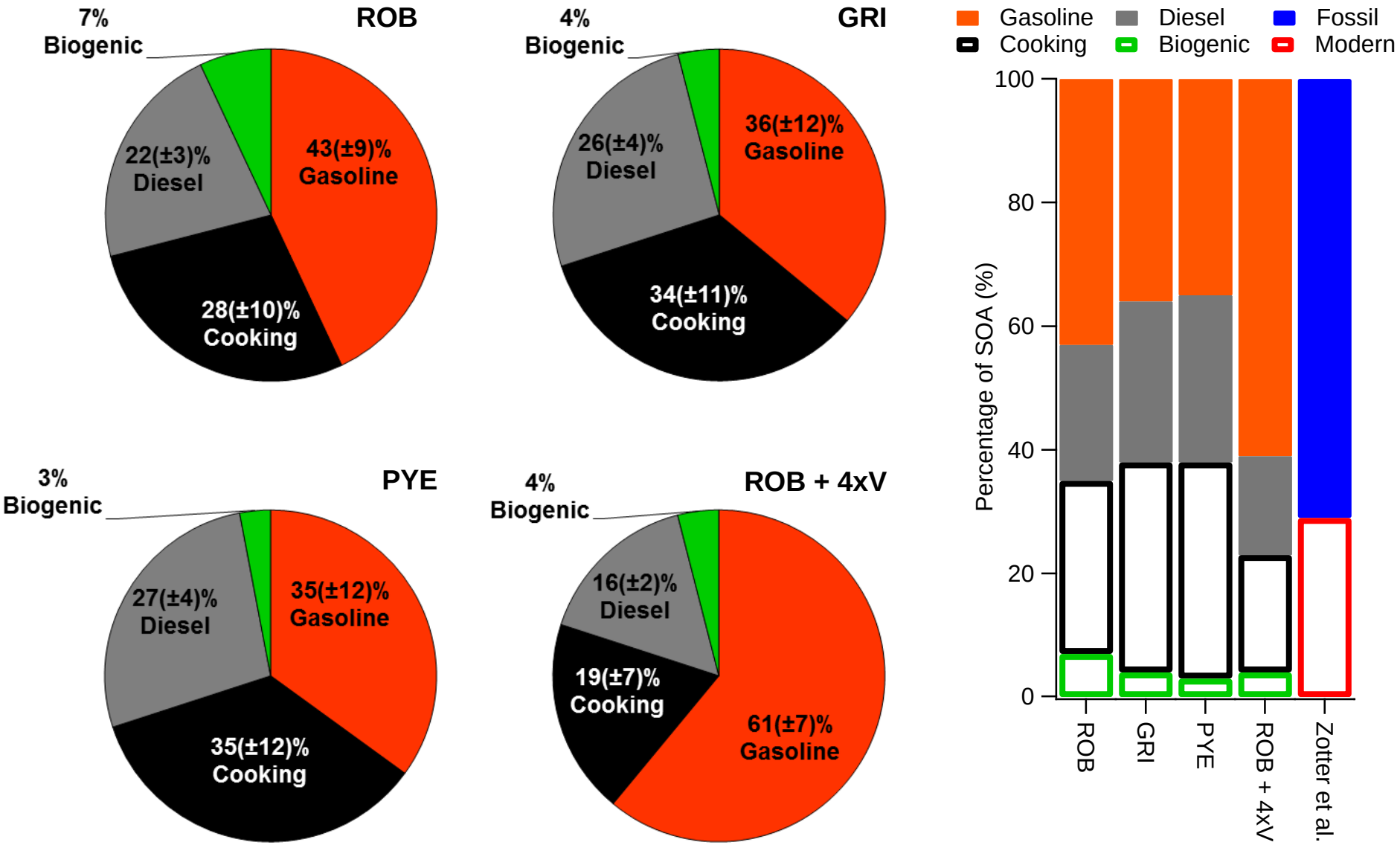
ROB
7% Biogenic
43(±9)% Gasoline
22(±3)% Diesel
28(±10)% Cooking
GRI
4% Biogenic
36(±12)% Gasoline
26(±4)% Diesel
34(±11)% Cooking
PYE
3% Biogenic
35(±12)% Gasoline
27(±4)% Diesel
35(±12)% Cooking
ROB + 4xV
4% Biogenic
61(±7)% Gasoline
16(±2)% Diesel
19(±7)% Cooking
Gasoline
Diesel
Fossil
Cooking
Biogenic
Modern
Percentage of SOA (%)
0
20
40
60
80
100
ROB
GRI
PYE
ROB + 4xV
Zotter et al.

Figure 6

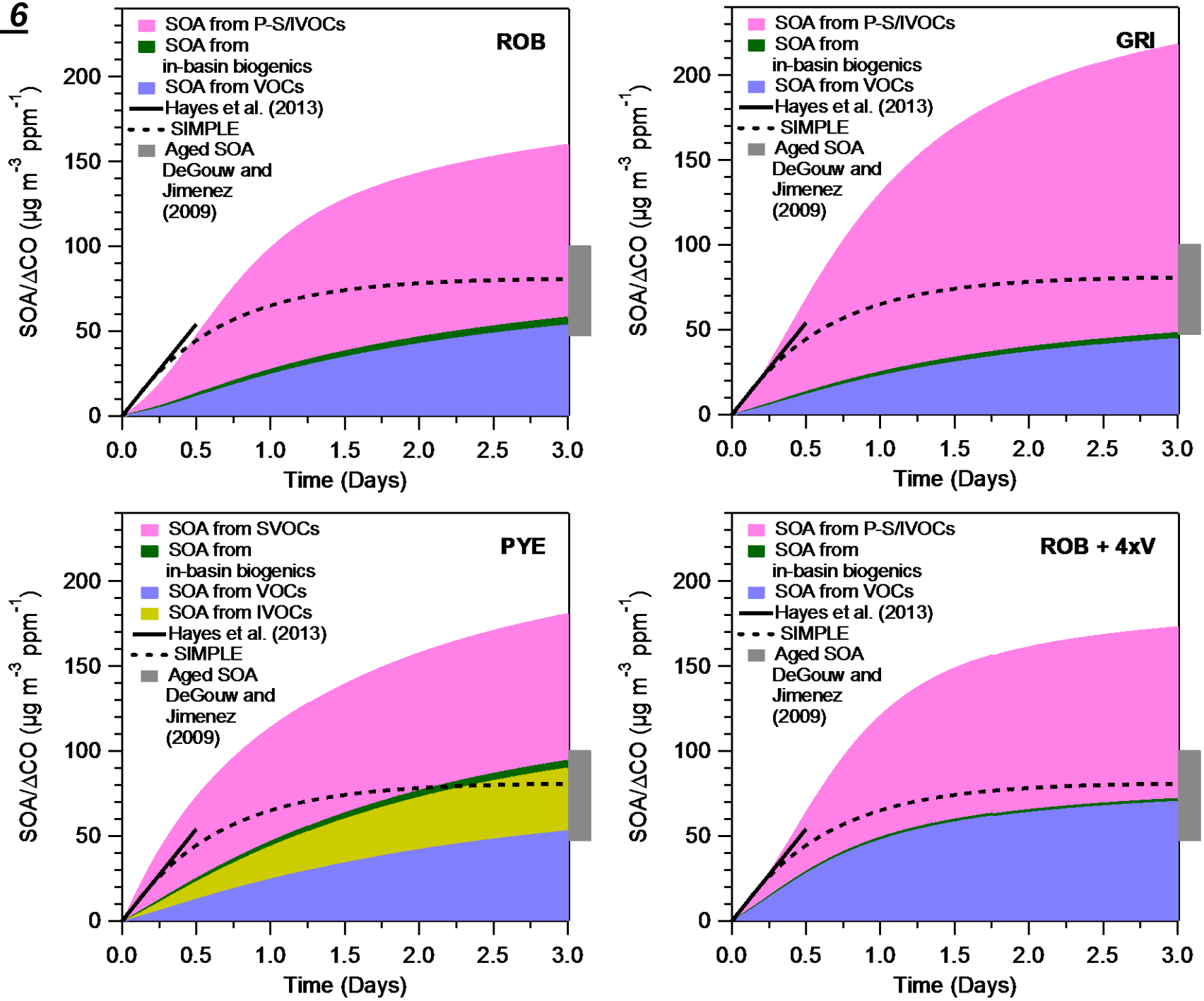
ROB
SOA from P-S/IVOCs
SOA from in-basin biogenics
SOA from VOCs
Hayes et al. (2013)
SIMPLE
Aged SOA DeGouw and Jimenez (2009)
GRI
PYE
SOA from SVOCs
SOA from IVOCs
ROB + 4xV
SOA/ΔCO (μg m-3 ppm-1)
Time (Days)
0
50
100
150
200
0.0
0.5
1.0
1.5
2.0
2.5
3.0

Figure 7

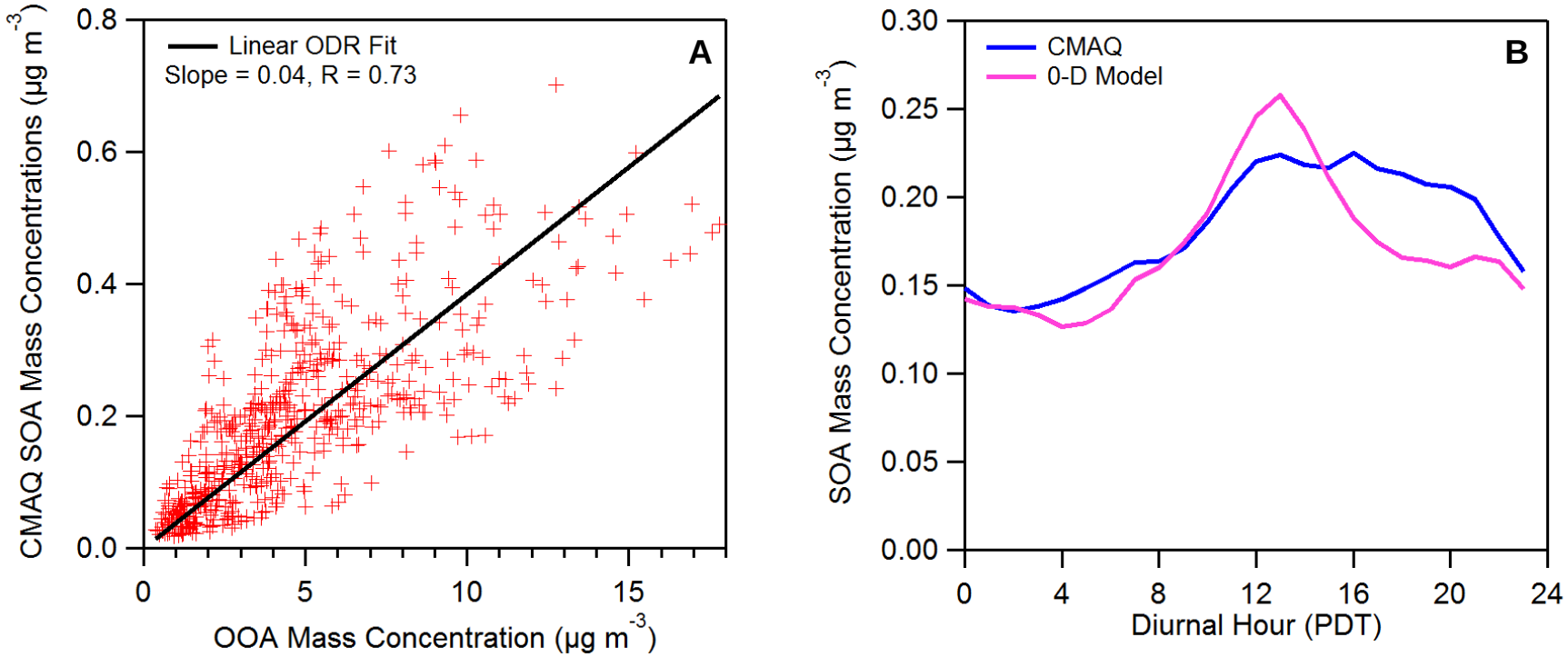
Linear ODR Fit
Slope = 0.04, R = 0.73
A
CMAQ SOA Mass Concentrations (µg m-3)
OOA Mass Concentration (µg m-3)
0.0
0.2
0.4
0.6
0.8
0
5
10
15
CMAQ
0-D Model
B
SOA Mass Concentration (µg m-3)
Diurnal Hour (PDT)
0.00
0.05
0.10
0.15
0.20
0.25
0.30
0
4
8
12
16
20
24

Figure 8

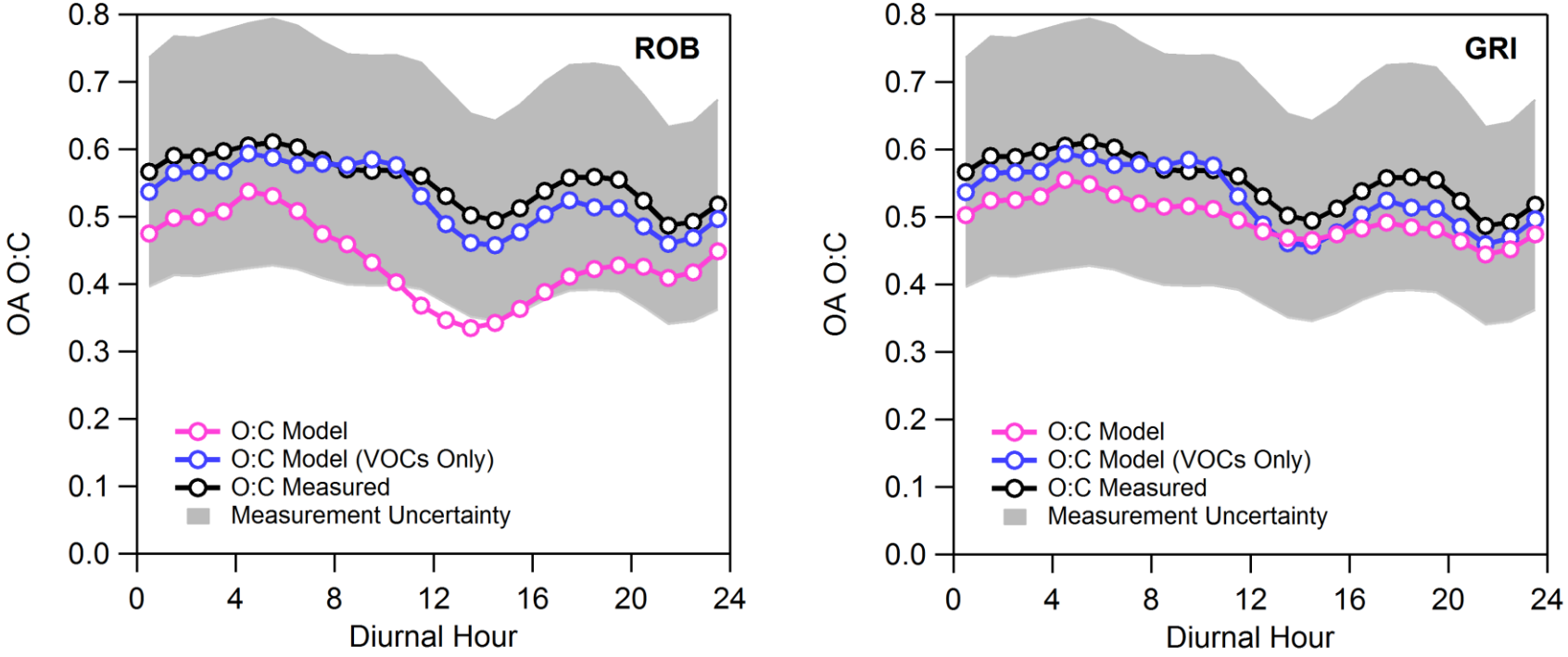
ROB
GRI
OA O:C
Diurnal Hour
0.0
0.1
0.2
0.3
0.4
0.5
0.6
0.7
0.8
0
4
8
12
16
20
24
O:C Model
O:C Model (VOCs Only)
O:C Measured
Measurement Uncertainty

Figure 9

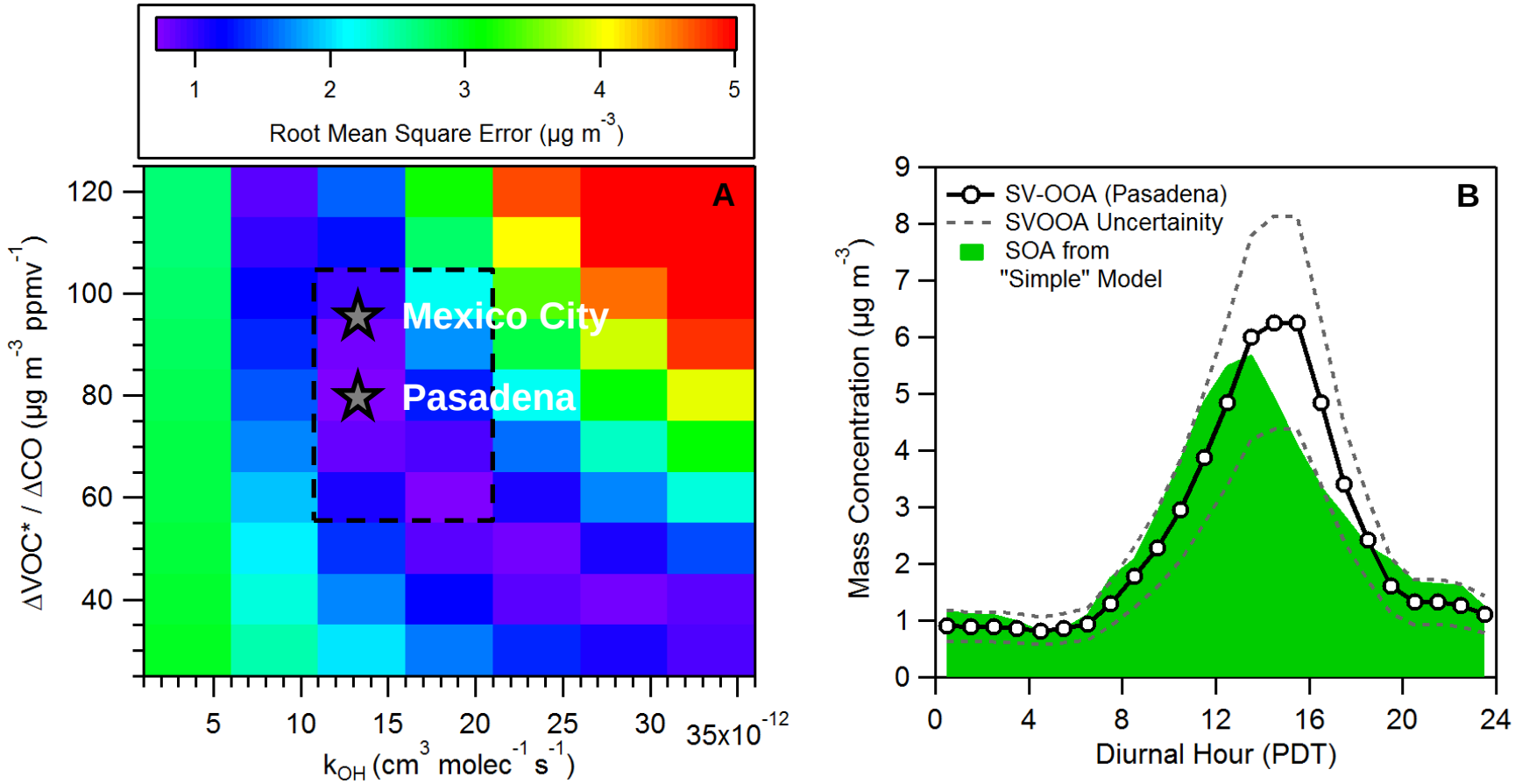
Root Mean Square Error (μg m-3)
1
2
3
4
5
A
Mexico City
Pasadena
ΔVOC* / ΔCO (μg m-3 ppmv-1)
120
100
80
60
40
5
10
15
20
25
30
35x10-12
kOH (cm3 molec-1 s-1)
B
SV-OOA (Pasadena)
SVOOA Uncertainity
SOA from
"Simple" Model
Mass Concentration (μg m-3)
0
1
2
3
4
5
6
7
8
9
0
4
8
12
16
20
24
Diurnal Hour (PDT)

Figure 10

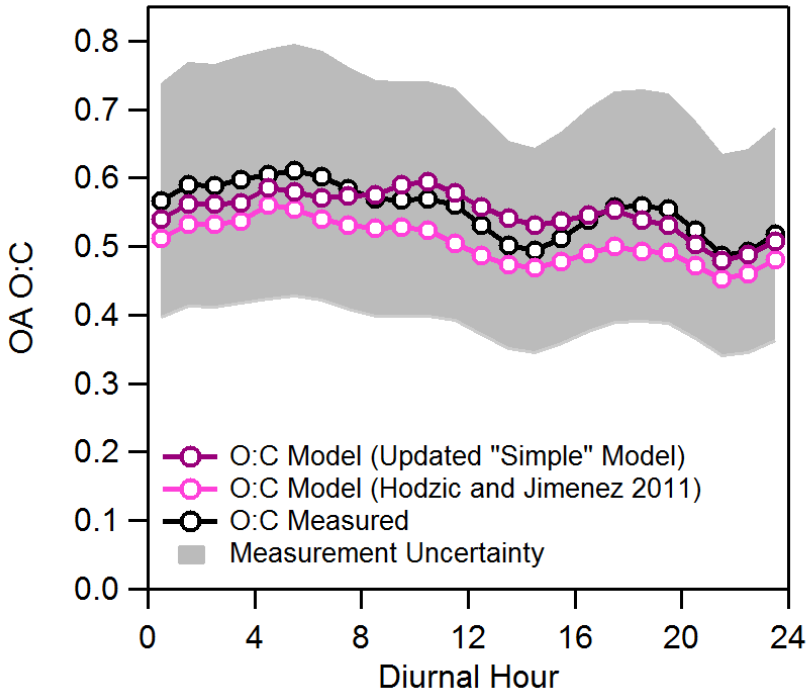
0.8
0.7
0.6
0.5
0.4
0.3
0.2
0.1
0.0
OA O:C
O:C Model (Updated "Simple" Model)
O:C Model (Hodzic and Jimenez 2011)
O:C Measured
Measurement Uncertainty
0
4
8
12
16
20
24
Diurnal Hour

Table SI-1

Precursor Family Name	Compounds	k_{OH} (cm^3 $molec^{-1}$ s^{-1})	ΔVOC/ΔCO (ppt ppb^{-1})	Stoichiometric SOA yield High-NO_X, 298 K, (μg m^{-3})				Molecular Weight (g mol^{-1})
				1	10	100	1000	
ALK5	Methylcyclopentane	5.68×10^{-12}	0.566	0.000	0.015	0.000	0.000	150
	Cyclohexane	6.97×10^{-12}	0.285					
	Methylcyclohexane	9.64×10^{-12}	0.202					
	n-Heptane	6.76×10^{-12}	0.398					
	2-Methyl Hexane	6.89×10^{-12}	0.385					
	3-Methyl Hexane	7.17×10^{-12}	0.460					
	2,3-Dimethyl Pentane	7.15×10^{-12}	0.252					
	2,4-Dimethyl Pentane	4.77×10^{-12}	0.171					
	2,2,3-Trimethyl Butane	3.81×10^{-12}	0.031					
	N-Octane	8.11×10^{-12}	0.197					
	3-Methyl Heptane	8.59×10^{-12}	0.131					
	2-Methyl Heptane	8.31×10^{-12}	0.171					
	2,2,4-Trimethyl Pentane	3.34×10^{-12}	0.476					
	2,3,4-Trimethyl Pentane	6.60×10^{-12}	0.171					
	2,3,3-Trimethyl Pentane	4.40×10^{-12}	0.194					
	N-Nonane	9.70×10^{-12}	0.220					
	N-Decane	11.0×10^{-12}	0.180					
	Undecane	12.3×10^{-12}	0.290					

Table SI-1 (cont.)

Precursor Family Name	Compounds	k_{OH} (cm^3 $molec^{-1}$ s^{-1})	ΔVOC/ΔCO (ppt ppb^{-1})	Stoichiometric SOA yield High-NO_X, 298 K, (μg m^{-3})				Molecular Weight (g mol^{-1})
				1	10	100	1000	
OLE1	Propene	26.3×10^{-12}	3.740	0.001	0.005	0.038	0.150	120
	1-Butene	31.4×10^{-12}	0.340					
	1-Pentene	31.4×10^{-12}	0.112					
	2-methyl-1-butene	61.0×10^{-12}	0.250					
	3-methyl-1-butene	31.8×10^{-12}	0.058					
OLE2	1,3-Butadiene	66.6×10^{-12}	0.350	0.003	0.026	0.083	0.27	120
	trans-2-Pentene	67.0×10^{-12}	0.097					
	cis-2-Pentene	65.0×10^{-12}	0.050					
	Styrene	58.0×10^{-12}	0.220					
ARO1	Toluene	5.63×10^{-12}	3.180	0.003	0.165	0.300	0.435	150
	Ethylbenzene	7.00×10^{-12}	0.570					
	i-Propylbenzene	6.30×10^{-12}	0.030					
	n-Propylbenzene	5.80×10^{-12}	0.110					
	Benzene	1.22×10^{-12}	1.300					
ARO2	o-Ethyltoluene	9.57×10^{-12}	0.120	0.002	0.195	0.300	0.435	150
	1,2,3-Trimethylbenzene	11.9×10^{-12}	0.240					
	1,2,4-Trimethylbenzene	32.7×10^{-12}	0.620					
	1,3,5-Trimethylbenzene	32.5×10^{-12}	0.310					
	m-xylene	56.7×10^{-12}	1.790					
	p-xylene	23.1×10^{-12}	1.790					

Table SI-1 (cont.)

Precursor Family Name	Compounds	k_{OH} (cm^3 $molec^{-1}$ s^{-1})	ΔVOC/ΔCO (ppt ppb^{-1})	Stoichiometric SOA yield High-NO_X, 298 K, (μg m^{-3})				Molecular Weight (g mol^{-1})
				1	10	100	1000	
NAPH	Naphthalene	24.4×10^{-12}	0.065	0.165	0.005	0.516	0.881	150
	1-Methylnaphthalene	40.9×10^{-12}	0.01					
	2-Methylnaphthalene	48.6×10^{-12}	0.021					
ISOP	Isoprene (Anthropogenic)	100×10^{-12}	N/A (see text)	0.001	0.023	0.015	0.000	136
	Isoprene (Biogenic)	100×10^{-12}	N/A (see text)					
TERP	α-Pinene + β-Pinene + Limonene	98.2×10^{-12}	N/A (see text)	0.012	0.122	0.201	0.5	180

Table SI-2

c* **@ 300 K (μg m^{-3})**	***ΔH$_{vap}$* (kJ mol^{-1})**		**Molecular Weight (g mol^{-1})**		**Fraction of total P-S/IVOC (%)**
ROB & GRI	ROB	GRI	ROB	GRI	ROB & GRI
0.01	112	77	250	524	1.2
0.1	106	73	250	479	2.4
1	100	69	250	434	3.6
10	94	65	250	389	5.6
100	88	61	250	344	7.2
1,000	82	57	250	299	12
10,000	76	54	250	254	16
100,000	70	50	250	208	20
1,000,000	64	46	250	163	32

	ROB	**GRI**
k_{OH} at 300 K (cm^3 molec^{-1} s^{-1})	4×10^{-11}	2×10^{-11}
Oxygen gain per oxidation generation (%)	1.075	1.4
Volatility bin decrease per oxidation generation	1 order of magnitude	2 orders of magnitude

Table SI-3

Tracer Molecule	**Precursors**	**Reference**
2-Methylglyceric acid	Isoprene	Edney et al. *Atmos. Environ.* **2005,** 5281-5289.
2-Methylthreitol	Isoprene	Edney et al. *Atmos. Environ.* **2005,** 5281-5289.
2-Methylerythritol	Isoprene	Edney et al. *Atmos. Environ.* **2005,** 5281-5289.
3-Acetyl pentanedioic acid	Monoterpenes	Jaoui et al. *Environ. Sci. Technol.* **2005,** 5661-5673.
3-Acetyl hexanedioic acid	Monoterpenes	Jaoui et al. *Environ. Sci. Technol.* **2005,** 5661-5673.
3-Methyl-1,2,3-butanetricarboxylic acid	Monoterpenes	Szmigielski et al. *J. Geophys. Res.-Atmos.* **2007,** L24811.
3-Hydroxyglutaric acid	Monoterpenes	Claeys et al. *Environ. Sci. Technol.* **2005,** 1628-1634.
3-Hydroxy-4,4-dimethylglutaric acid	Monoterpenes	Claeys et al. *Environ. Sci. Technol.* **2005,** 1628-1634.
Pinic acid	Monoterpenes	Claeys et al. *Environ. Sci. Technol.* **2005,** 1628-1634.

Figure SI-1

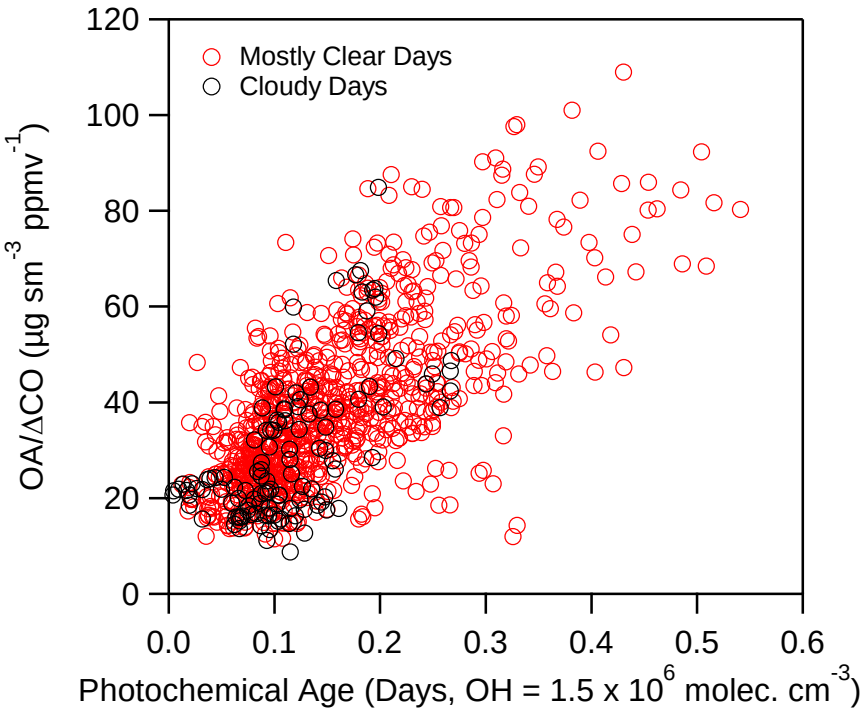
Mostly Clear Days
Cloudy Days
OA/ΔCO (µg sm^{-3} ppmv^{-1})
0
20
40
60
80
100
120
0.0
0.1
0.2
0.3
0.4
0.5
0.6
Photochemical Age (Days, OH = 1.5 x 10^{6} molec. cm^{-3})

Figure SI-2

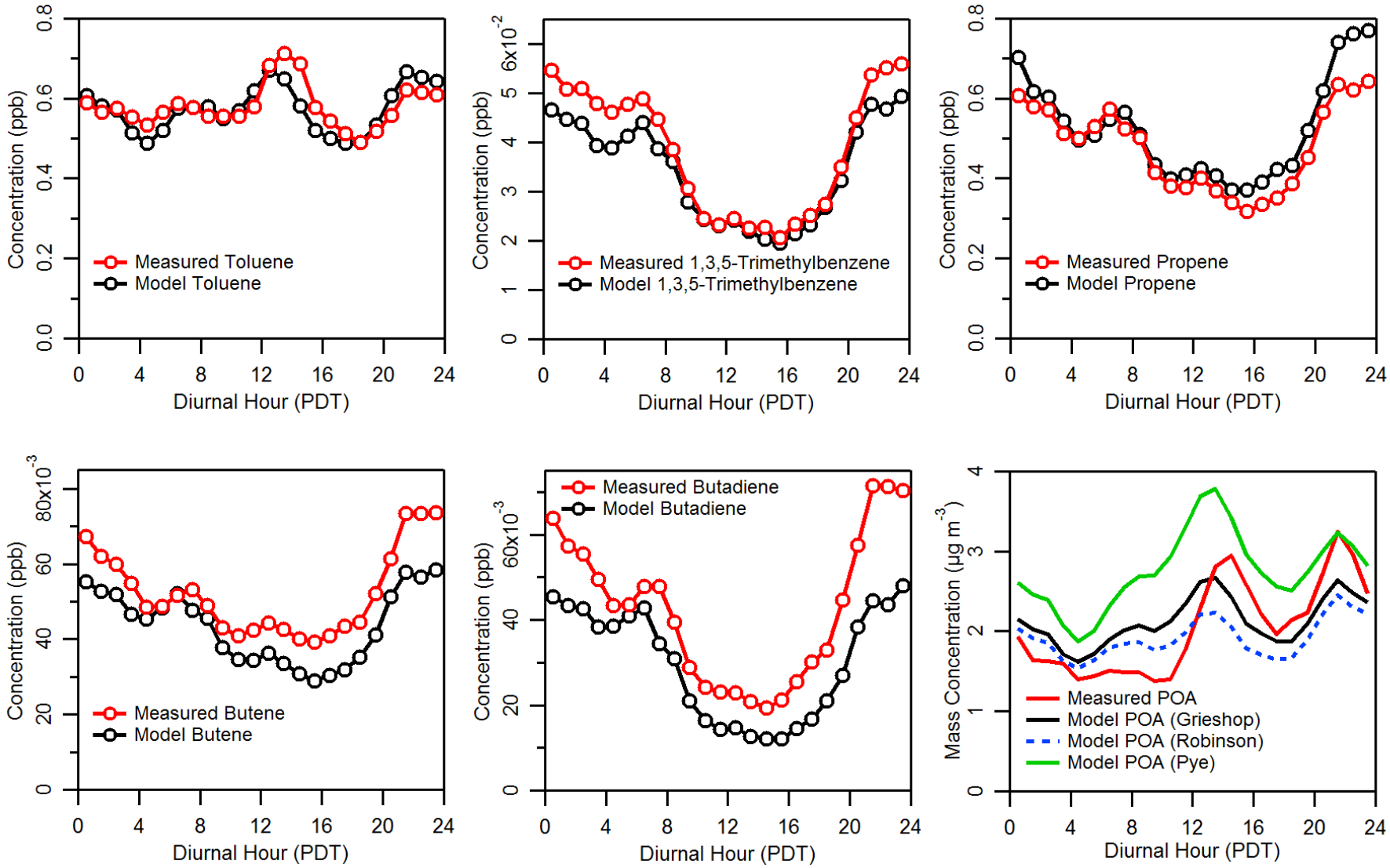
Concentration (ppb)
Diurnal Hour (PDT)
Measured Toluene
Model Toluene
Measured 1,3,5-Trimethylbenzene
Model 1,3,5-Trimethylbenzene
Measured Propene
Model Propene
Measured Butene
Model Butene
Measured Butadiene
Model Butadiene
Mass Concentration (μg m-3)
Measured POA
Model POA (Grieshop)
Model POA (Robinson)
Model POA (Pye)

Figure SI-3

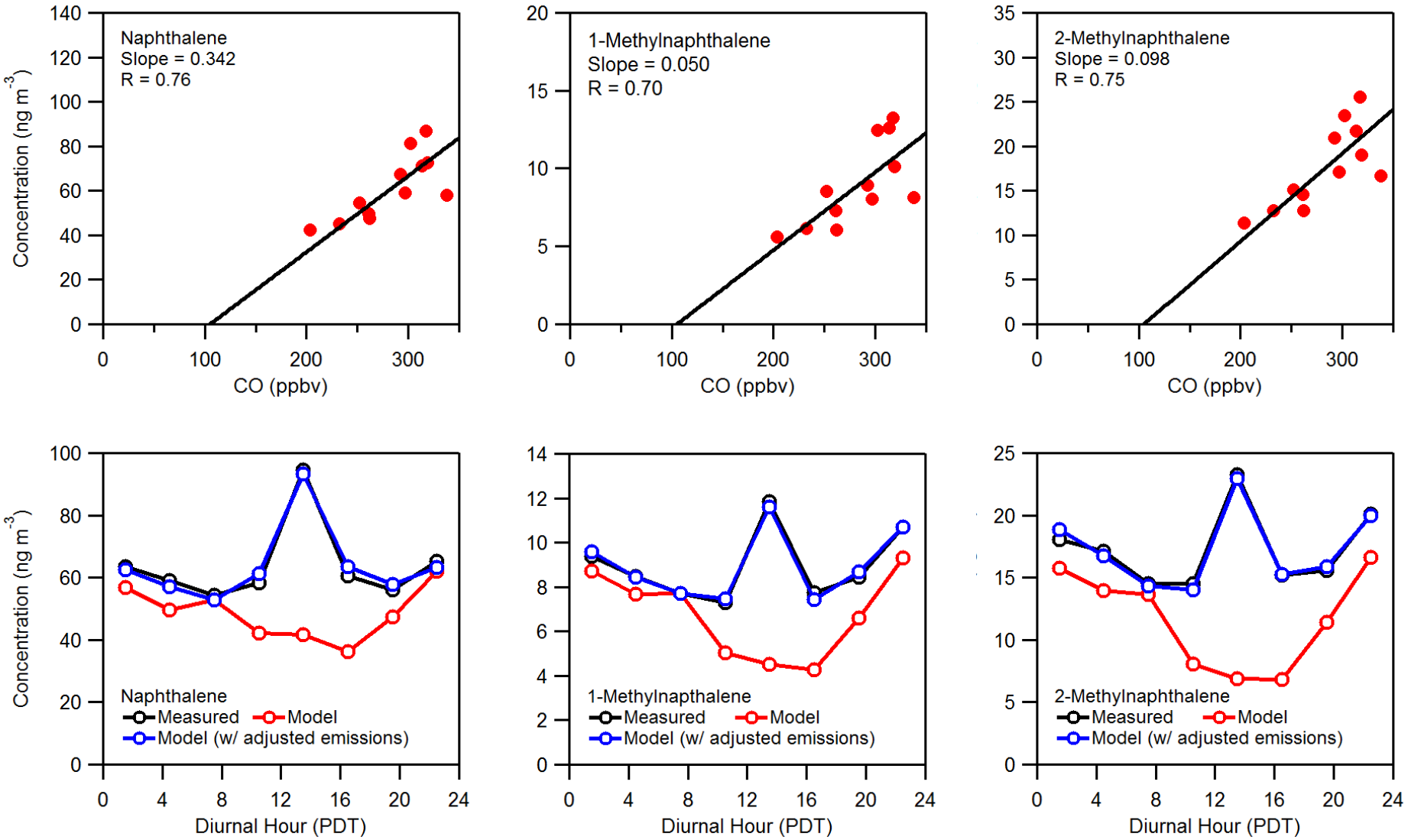
Naphthalene
Slope = 0.342
R = 0.76
1-Methylnaphthalene
Slope = 0.050
R = 0.70
2-Methylnaphthalene
Slope = 0.098
R = 0.75
Concentration (ng m-3)
CO (ppbv)
Diurnal Hour (PDT)
Measured
Model
Model (w/ adjusted emissions)

Figure SI-4

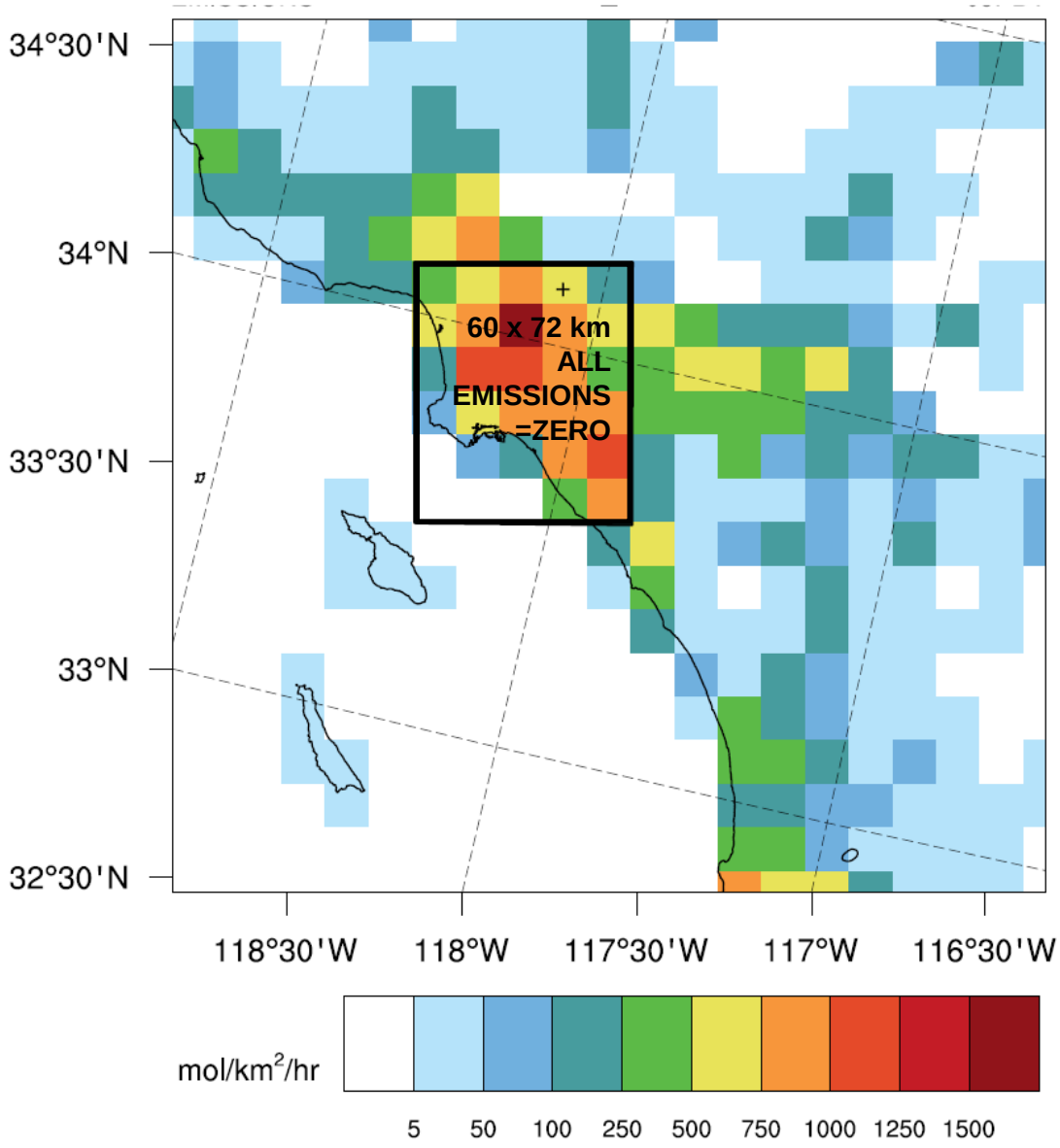
34°30'N
34°N
33°30'N
33°N
32°30'N
118°30'W
118°W
117°30'W
117°W
116°30'W
60 x 72 km
ALL
EMISSIONS
=ZERO
mol/km²/hr
5
50
100
250
500
750
1000
1250
1500

Figure SI-5

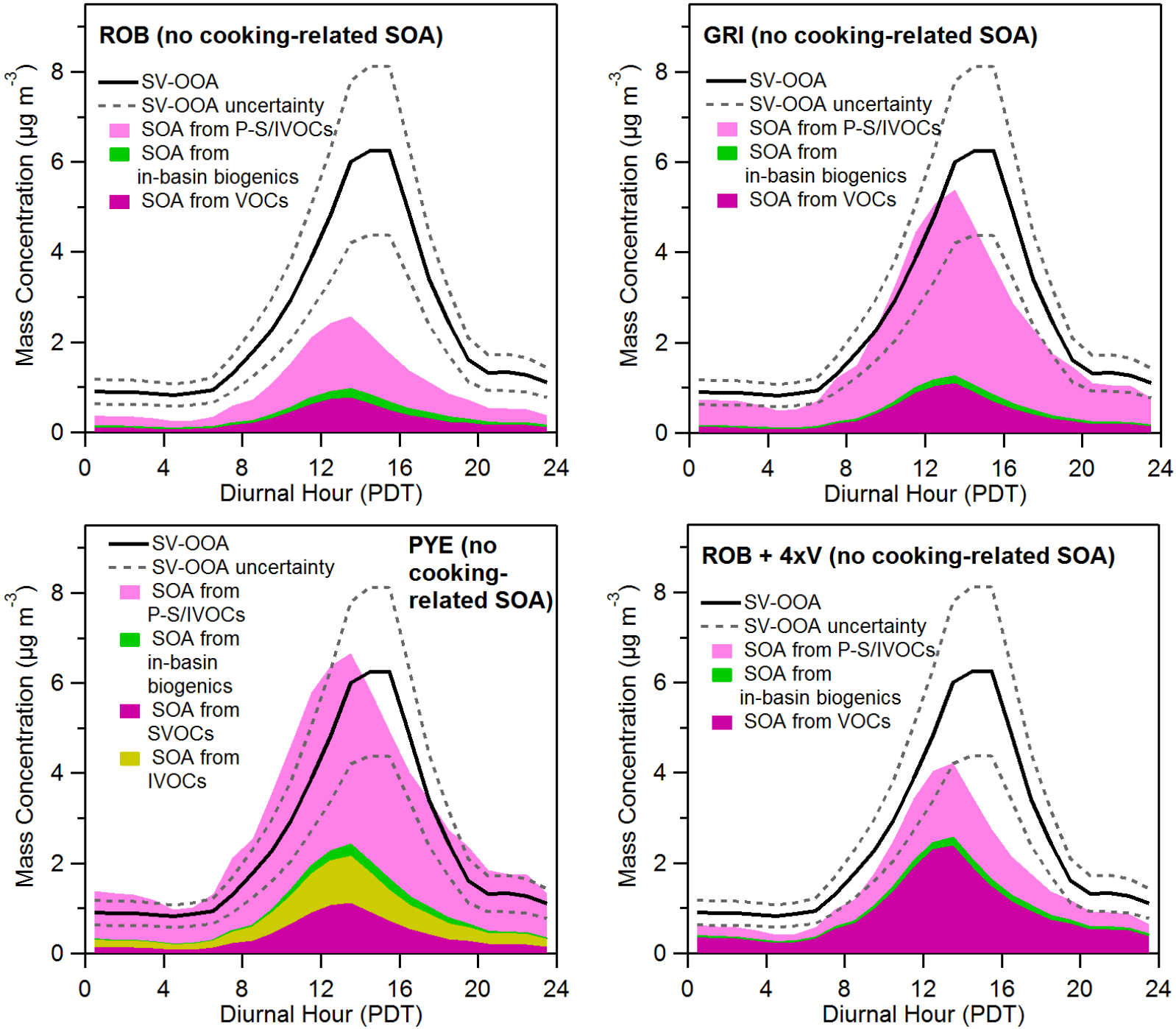
ROB (no cooking-related SOA)
SV-OOA
SV-OOA uncertainty
SOA from P-S/IVOCs
SOA from in-basin biogenics
SOA from VOCs
GRI (no cooking-related SOA)
SV-OOA
SV-OOA uncertainty
SOA from P-S/IVOCs
SOA from in-basin biogenics
SOA from VOCs
PYE (no cooking-related SOA)
SV-OOA
SV-OOA uncertainty
SOA from P-S/IVOCs
SOA from in-basin biogenics
SOA from SVOCs
SOA from IVOCs
ROB + 4xV (no cooking-related SOA)
SV-OOA
SV-OOA uncertainty
SOA from P-S/IVOCs
SOA from in-basin biogenics
SOA from VOCs
Mass Concentration (μg m-3)
Diurnal Hour (PDT)
0
2
4
6
8
0
4
8
12
16
20
24

Figure SI-6

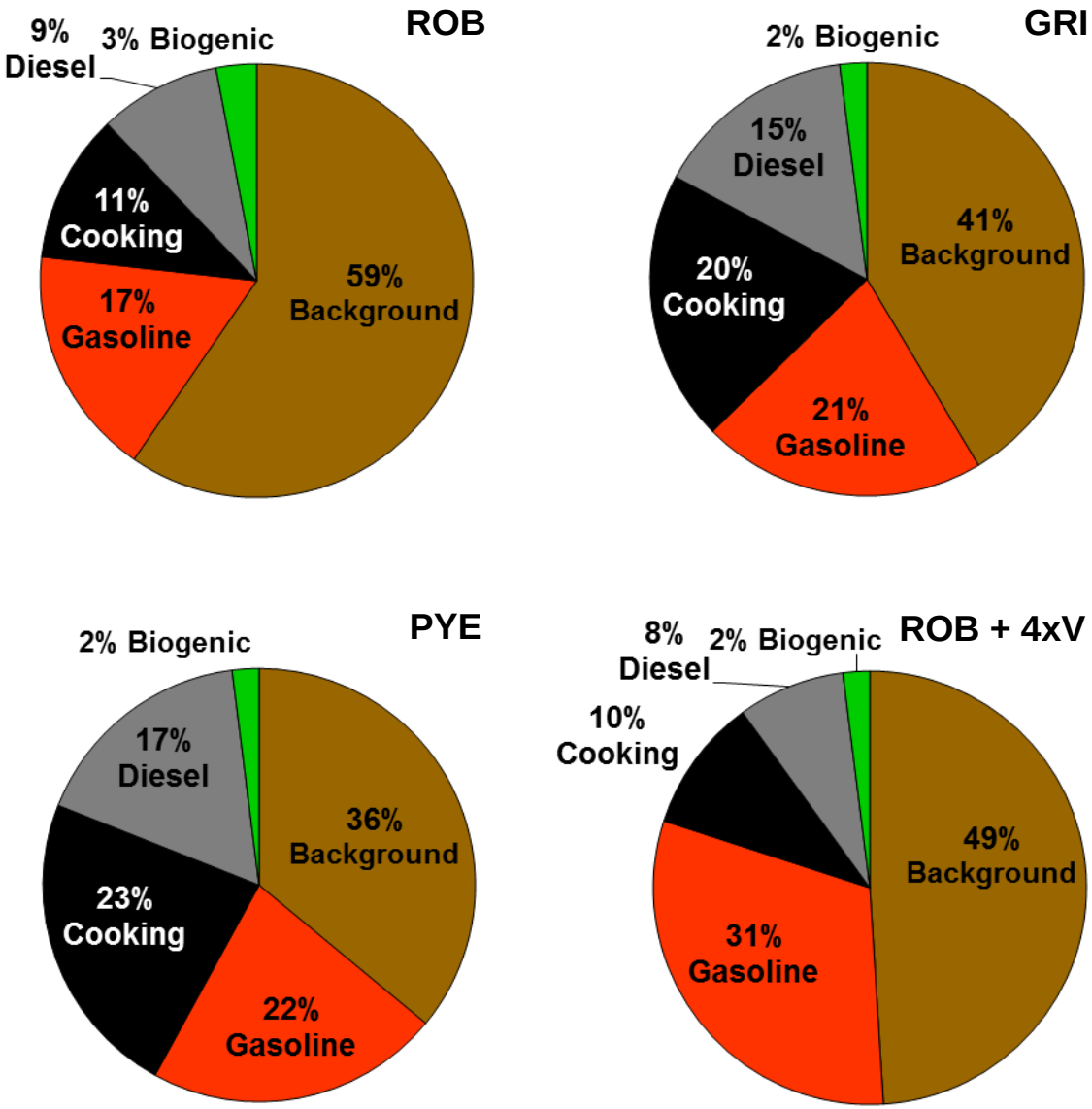
ROB
9% Diesel
3% Biogenic
11% Cooking
17% Gasoline
59% Background
GRI
2% Biogenic
15% Diesel
20% Cooking
21% Gasoline
41% Background
PYE
2% Biogenic
17% Diesel
23% Cooking
22% Gasoline
36% Background
ROB + 4xV
8% Diesel
2% Biogenic
10% Cooking
31% Gasoline
49% Background

Figure SI-7

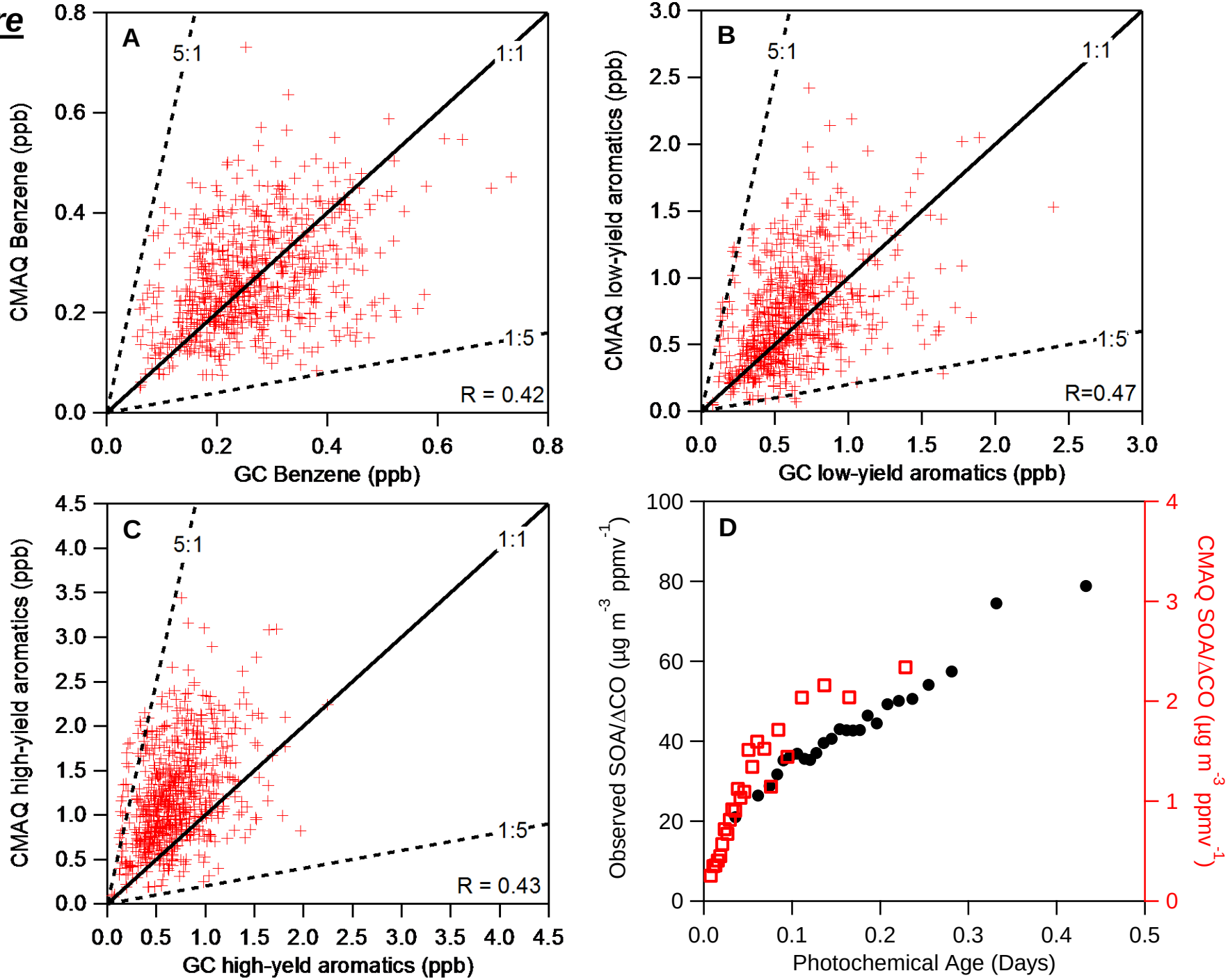
A
5:1
1:1
1:5
R = 0.42
CMAQ Benzene (ppb)
GC Benzene (ppb)
B
5:1
1:1
1:5
R=0.47
CMAQ low-yield aromatics (ppb)
GC low-yield aromatics (ppb)
C
5:1
1:1
1:5
R = 0.43
CMAQ high-yield aromatics (ppb)
GC high-yeld aromatics (ppb)
D
Observed SOA/ΔCO (μg m-3 ppmv-1)
CMAQ SOA/ΔCO (μg m-3 ppmv-1)
Photochemical Age (Days)

Figure SI-8

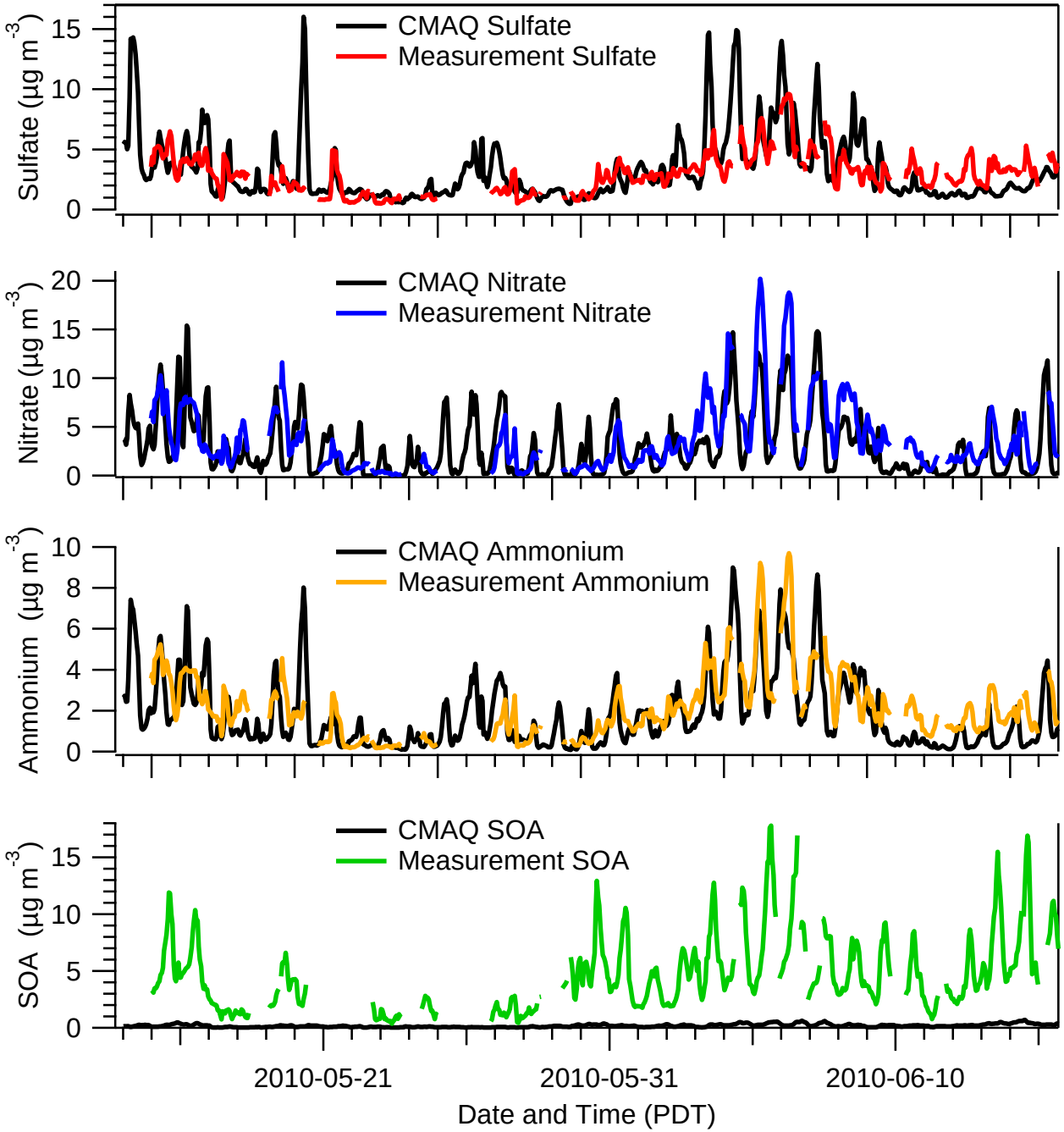
CMAQ Sulfate
Measurement Sulfate
Sulfate (µg m-3)
0
5
10
15
CMAQ Nitrate
Measurement Nitrate
Nitrate (µg m-3)
0
5
10
15
20
CMAQ Ammonium
Measurement Ammonium
Ammonium (µg m-3)
0
2
4
6
8
10
CMAQ SOA
Measurement SOA
SOA (µg m-3)
0
5
10
15
2010-05-21
2010-05-31
2010-06-10
Date and Time (PDT)

Figure SI-9

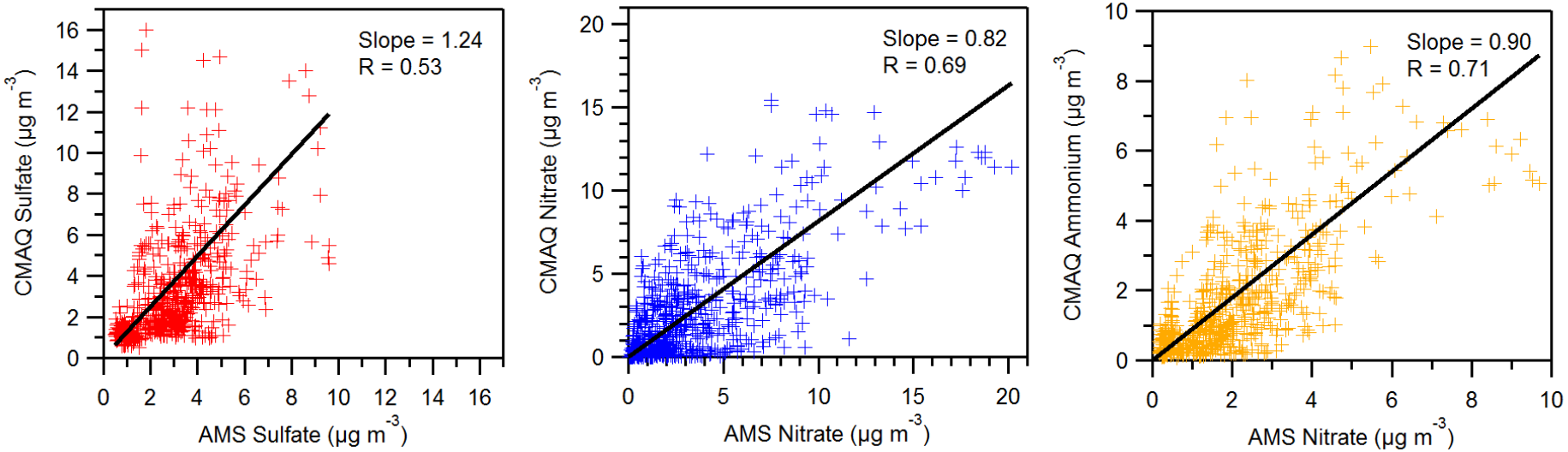
Slope = 1.24
R = 0.53
CMAQ Sulfate (μg m-3)
AMS Sulfate (μg m-3)
Slope = 0.82
R = 0.69
CMAQ Nitrate (μg m-3)
AMS Nitrate (μg m-3)
Slope = 0.90
R = 0.71
CMAQ Ammonium (μg m-3)
AMS Nitrate (μg m-3)